

Paleoceanography and Paleoclimatology

RESEARCH ARTICLE

10.1029/2020PA004153

Key Points:

- First ϵNd record of the central Mediterranean Sea during the last climatic cycle
- Reconstruction of water exchanges variations between the eastern and western Mediterranean basins during the last climatic cycle
- Evidence of millennial-scale variations of ϵNd during the last glacial time indicating pulses of LIW intrusion into the Tyrrhenian Sea

Supporting Information:

Supporting Information may be found in the online version of this article.

Correspondence to:

C. Colin,
christophe.colin@universite-paris-saclay.fr









Citation:

Colin, C., Duhamel, M., Siani, G., Dubois-Dauphin, Q., Ducassou, E., Liu, Z., et al. (2021). Changes in the intermediate water masses of the Mediterranean Sea during the last climatic cycle—New constraints from neodymium isotopes in foraminifera. *Paleoceanography and Paleoclimatology*, 36, e2020PA004153. <https://doi.org/10.1029/2020PA004153>

Received 30 OCT 2020
 Accepted 31 JAN 2021

© 2021. American Geophysical Union.
 All Rights Reserved.

Changes in the Intermediate Water Masses of the Mediterranean Sea During the Last Climatic Cycle—New Constraints From Neodymium Isotopes in Foraminifera

Christophe Colin¹ , Maxence Duhamel¹, Giuseppe Siani¹ , Quentin Dubois-Dauphin¹ , Emmanuelle Ducassou², Zhifei Liu³ , Jiawang Wu³ , Marie Revel⁴, Arnaud Dapoigny⁵, Eric Douville⁵ , Marco Taviani^{6,7,8} , and Paolo Montagna^{9,10} 

¹Université Paris-Saclay, CNRS, GEOPS, Orsay, France, ²Université de Bordeaux, UMR-CNRS 5805-EPOC, Pessac Cedex, France, ³State Key Laboratory of Marine Geology, Tongji University, Shanghai, China, ⁴Université de la Côte d'Azur, CNRS, OCA, IRD, Geoazur, Valbonne, France, ⁵Laboratoire des Sciences du Climat et de l'Environnement, LSCE/IPSL, CEA-CNRS-UVSQ, Université Paris-Saclay, France, ⁶Institute of Marine Science, ISMAR-CNR, Bologna, Italy, ⁷Stazione Zoologica Anton Dohrn, Naples, Italy, ⁸Biology Department, Woods Hole Oceanographic Institution, Woods Hole, MA, USA, ⁹Institute of Polar Sciences, ISP-CNR, Bologna, Italy, ¹⁰Lamont Doherty Earth Observatory, Columbia University, Palisades, NY, USA

Abstract Variations in Mediterranean thermohaline circulation of the Quaternary are still not well constrained whereas they have been considered to have an influence on the Atlantic Meridional Overturning Circulation and on the oxygenation of waters in the deep basins of the Mediterranean Sea. ϵNd analyses have been carried out on planktonic foraminifera of cores collected in the central Mediterranean Sea to constrain water mass exchange between the Eastern and Western Mediterranean Sea (EMS and WMS) during the last climatic cycle. ϵNd records from the WMS and EMS display similar higher values during warm substages of interglacial Marine Isotopic Stage (MIS) 1 and 5. This suggests an efficient connection between the two Mediterranean sub-basins and the transfer of radiogenic waters to the Tyrrhenian Sea via the Levantine Intermediate Water (LIW). Conversely, during glacial MIS, ϵNd of the intermediate depth of the Tyrrhenian Sea are less radiogenic than the EMS, implying limited hydrological connection between sub-basins during low sea-level stands. Superimposed on these glacial-interglacial variations, increased ϵNd occurred during Heinrich Stadial events. This suggests a reduction in the formation of unradiogenic WIW in the Gulf of Lions due to the input of relatively fresh surface Atlantic water to the WMS and/or the inflow of radiogenic glacial LIW and upper EMDW to the Tyrrhenian Sea as a result of an active EMS convection related to saltier and colder conditions. Such potential millennial-scale pulses of LIW intrusion into the Tyrrhenian Sea may have led to an enhanced Mediterranean Outflow Water intensity in the Gibraltar Strait.

1. Introduction

The Mediterranean Sea is a semi-enclosed basin characterized by arid conditions and connected to the North Atlantic through the Strait of Gibraltar (sill depth of ~ 300 m). This generates a Mediterranean thermohaline circulation where the inflow of relatively fresh and cold surface Atlantic water (AW) is transformed into intermediate and deep waters in the Gulf of Lions, the Adriatic Sea, the Levantine Basin and the Aegean Sea (Robinson et al., 2001; Schroeder et al., 2012). In particular, the Levantine Intermediate Water (LIW) is formed in the Cyprus-Rhodes area from where it spreads westwards into the entire Mediterranean Sea at water depths of between ~ 150 and 700 m (Lascaratos et al., 1993; Malanotte-Rizzoli et al., 1999). This overturning circulation is associated with an outflow of saltier and warmer intermediate water into the North Atlantic corresponding to the Mediterranean Outflow Water (MOW) (Robinson et al., 2001; Schroeder et al., 2012). Because the MOW contains up to $\sim 80\%$ of LIW, the water mass formation in the Levantine Sea plays an important role for the salty outflow to the North Atlantic through the Strait of Gibraltar. A link between the intensification of the MOW and the intensity of the Atlantic Meridional Overturning Circulation (AMOC) has been proposed (Bahr et al., 2015; Cacho et al., 1999, 2000, 2001; Rogerson et al., 2005, 2010, 2012; Sierrro et al., 2005; Voelker et al., 2006).

Past variations in Mediterranean thermohaline circulation were highly sensitive to climate changes at both high and low latitudes of the Northern Hemisphere (e.g., Bahr et al., 2015; Emeis et al., 2003; Filippidi et al., 2016; Frigola et al., 2008; Kallel et al., 1997; Melki et al., 2009; Revel et al., 2010; Rossignol-Strick et al., 1982; Rohling et al., 2002; Scrivner et al., 2004; Toucanne et al., 2015; Tesi et al., 2017) and have been associated with the deposition of organic-rich layers (ORLs) in the Western Mediterranean Sea (WMS) and of sapropels in the Eastern Mediterranean Sea (EMS) (e.g., Filippidi et al., 2016; Tachikawa et al., 2015; Tesi et al., 2017).

Previous work has shown that changes in Mediterranean thermohaline circulation (Filippidi et al., 2016; Tachikawa et al., 2015; Tesi et al., 2017) are mainly induced by freshwater input from the heavy monsoonal precipitation in North Africa channeled by the Nile River (Rossignol-Strick et al., 1982) and other North African paleo-rivers (e.g., Emeis et al., 2003; Fontugne et al., 1994; Rohling et al., 2002; Rossignol-Strick et al., 1982; Revel et al., 2010). Increased runoff is associated with a stronger, nutrient-rich, freshwater inflow into the Mediterranean Sea leading to higher surface productivity and water mass stratification in the EMS. In North Africa, these humid periods have been attributed to the northward migration of the rain belt associated with the Intertropical Convergence Zone (ITCZ) and related to precession-driven insolation changes (Arbuszewski et al., 2013; DeMenocal et al., 2000; Gasse, 2000; Rossignol-Strick et al., 1982; Skonieczny et al., 2019; Zaho et al., 2011, 2012). Hence, the deposition of organic-rich sapropel layers in the EMS is closely linked to: (1) higher productivity causing organic matter mineralization exceeding oxygen renewal; or (2) reduced ventilation (sluggish thermohaline circulation) caused by freshwater lowering surface salinity and stopping oxygen renewal; or (3) a combination of both processes (Cramp & O'Sullivan, 1999; Rohling, 1994; Rohling et al., 2015).

Several studies have shown that Mediterranean thermohaline circulation is sensitive to rapid climatic changes in the Northern Hemisphere (Allen et al., 1999; Bartov et al., 2003; Kallel et al., 1997; Martrat et al., 2004; Rohling et al., 1995). Modifications in Mediterranean Sea circulation occurred during the last glacial period, especially during the Heinrich and Dansgaard—Oeschger events of the North Atlantic, supporting the idea of a strong relationship between North Atlantic climate and the hydrology of the Mediterranean Sea (Cacho et al., 1999, 2000, 2001; Moreno et al., 2002, 2005; Paterne et al., 1999; Penaud et al., 2011; Rohling et al., 2002; Sierro et al., 2005; Toucanne et al., 2012; Voelker et al., 2006). It has been proposed that a decrease in the salinity of the North Atlantic during the Heinrich Stadial 1 (HS1) could have played a role in the surface salinity budget of the Mediterranean Sea (Sierro et al., 2005). Moreover, it has been suggested that variations in the salinity of the Atlantic Water flowing into the Mediterranean Sea, combined with changes in the water mass exchanges through the shallow Straits of Gibraltar and Sicily during sea level rise of the last Termination I, led to a drop in surface salinity (Cita et al., 1977; Emeis et al., 2000; Kallel et al., 1997; Williams & Thunell, 1979) thereby preconditioning sapropel formation by slowing down intermediate and deep water convection (Duhamel et al., 2020; Grimm et al., 2015).

Continuous $\delta^{13}\text{C}$ and $\delta^{18}\text{O}$ records of epibenthic foraminifera are scarce for the last glacial/interglacial climatic cycle due to the lack of epibenthic foraminifer species with calibrated vital effect for $\delta^{13}\text{C}$ analyses (Schmiedl et al., 2003, 2010) during bottom suboxic or anoxic events (e.g., sapropel events and ORLs). Here, we use the Nd isotopic composition, expressed as $\epsilon\text{Nd} = [({}^{143}\text{Nd}/{}^{144}\text{Nd})_{\text{sample}}/({}^{143}\text{Nd}/{}^{144}\text{Nd})_{\text{CHUR}} - 1] * 10,000$ (present-day $({}^{143}\text{Nd}/{}^{144}\text{Nd})_{\text{CHUR}}$ value of 0.512638; Jacobsen & Wasserburg, 1980), of diagenetic Fe-Mn coatings precipitated on foraminifer shells. It has been demonstrated that ϵNd measured on planktonic foraminifer shells mainly represents bottom seawater and/or pore water ϵNd (Tachikawa et al., 2013, 2014). The Nd residence time of 500–1,000 years (Siddall et al., 2008; Tachikawa et al., 2003) is shorter than the global turnover time of the ocean (about 1,000 years in the global ocean (Broecker, 1982) and shorter in the Mediterranean Sea). Consequently, through lithogenic inputs of material with various Nd isotopic signatures such as from boundary-exchange processes that occur at the continental margin (e.g., Lacan & Jean-del, 2005) and from benthic flux of Nd (Abbott et al., 2015; Du et al., 2018), intermediate- and deep-water masses acquire ϵNd from downwelling areas in the Mediterranean Sea. Modern seawater ϵNd values of the Mediterranean Sea range from -11 to -5 with unradiogenic Atlantic surface water and radiogenic intermediate and deep waters from the Levantine Sea acquired through water exchanges with particularly high radiogenic volcanic-sourced sediments on the eastern margins of the Levantine basin (Henry et al., 1994; Tachikawa et al., 2004; Vance et al., 2004). Away from the continental margins and on short time scales

(<500 years), ϵNd can serve as a water mass provenance tracer providing insight into water mass exchange between both Mediterranean Sea basins and with the adjacent North Atlantic (Cornuault et al., 2018; Dubois-Dauphin et al., 2017; Duhamel et al., 2020; Wu et al., 2019).

In this study, ϵNd has been analyzed on planktonic foraminifera from 5 cores located in the central and eastern Mediterranean Sea. The cores investigated here have been selected from both sides of the Strait of Sicily to trace past ϵNd variations of LIW and the underlying Western Mediterranean Deep Water (WMDW) in the western Mediterranean Sea. Reconstructed ϵNd values have been integrated with existing published records from the Levantine basin (Duhamel et al., 2020; Wu et al., 2019), the Strait of Sicily (Cornuault et al., 2018), the Ionian Sea (Wu et al., 2019), and the Alboran and Balearic Seas (Dubois-Dauphin et al., 2017; Jiménez-Espejo et al., 2015) in order to constrain water mass exchanges between the eastern and western Mediterranean basins over the last 145 kyr and constrain ϵNd of deep-water masses formed in the Adriatic Sea.

2. Hydrological Setting and Materials

2.1. Hydrological Setting

The relatively fresh surface AW (salinity < 36.5), which has an unradiogenic ϵNd signatures of ~ -11 (Spivack & Wasserburg, 1988; Tachikawa et al., 2004), flows into the WMS. During its eastward flow, AW mixes with the surrounding surface and underlying intermediate waters to form the Modified Atlantic Water (MAW) which follows a cyclonic, meandering flow path through the Mediterranean Sea at 50–200 m water depth (Figure 1). The ϵNd values for MAW range from -10.8 ± 0.4 to -8.8 ± 0.3 in the western basin (Dubois-Dauphin et al., 2017; Garcia-Solsona & Jeandel, 2020; Henry et al., 1994; Spivack & Wasserburg, 1988; Tachikawa et al., 2004) and from -9.3 ± 0.2 to -4.2 ± 0.2 in the eastern basin (Tachikawa et al., 2004; Vance et al., 2004) (Figure 1b). Since evaporation exceeds precipitation and river runoff, the relatively fresh surface AW flowing into the WMS also becomes progressively saltier (~ 38.5) as it flows eastward.

During winter, intense cooling and strong wind-induced heat loss produce denser waters that sink via convection to form intermediate waters in the Aegean Sea and the Levantine Basin and deep waters in the Gulf of Lions and the Adriatic Sea (Robinson et al., 2001; Schroeder et al., 2012) (Figure 1a). In particular, LIW, which is formed in the Cyprus-Rhodes area, acquires its Nd isotopic signature principally from the partial dissolution of radiogenic (from -3 to $+3$; Tachikawa et al., 2004) Nile River sediment discharge and radiogenic margin sediments of the Levantine Basin (Ayache et al., 2016; Blanchet, 2019; Castañeda et al., 2016; Weldeab et al., 2002) (Figure 1a). The ϵNd signature of LIW is -4.8 ± 0.4 in the eastern part of the EMS and gradually decreases westward to -6.5 ± 0.6 in the Levantine Sea, -7.7 ± 0.6 in the Strait of Sicily and -9.3 ± 0.7 in the Alboran Sea, through the mixing with overlying MAW and underlying unradiogenic water masses WIW/TDW (Dubois-Dauphin et al., 2017; Henry et al., 1994; Tachikawa et al., 2004; Vance et al., 2004) (Figure 1b).

In the Adriatic Sea, LIW participates in the formation of Adriatic Deep Water (AdDW) which flows into the deep Ionian Basin and contributes with Aegean Deep Water (AeDW) to the formation of Eastern Mediterranean Deep Water (EMDW) (e.g., Millot & Taupier-Letage, 2005) (Figure 1a). The ϵNd values of EMDW range from -7.3 ± 0.4 to -6.4 ± 0.8 (Tachikawa et al., 2004; Vance et al., 2004). The relatively fresh and cold MAW and saline LIW mix in winter to form WMDW in the Gulf of Lions, which spreads into the Balearic Basin and Tyrrhenian Sea between $\sim 2,000$ and $\sim 3,000$ m (Millot, 1999; Schroeder et al., 2012) (Figure 1a). The WMDW is characterized by ϵNd values ranging from -9.7 ± 0.6 in the Alboran Sea to -8.8 ± 0.5 in the Balearic Sea (Garcia-Solsona & Jeandel, 2020; Henry et al., 1994; Tachikawa et al., 2004) (Figure 1b). Tyrrhenian Deep Water (TDW) flows between the WMDW and the LIW, at depths from ~ 700 to $\sim 2,000$ m (Millot et al., 2006). Produced by the mixing of WMDW with a fraction of the EMDW outflowing through the Strait of Sicily, TDW has a mean ϵNd value of -8.3 ± 0.6 .

2.2. Samples Material

Planktonic foraminifera samples have been collected from 5 sediment cores in order to trace past changes in the Nd isotopic composition of the Intermediate- and deep-water masses on both sides of the Strait of Sicily

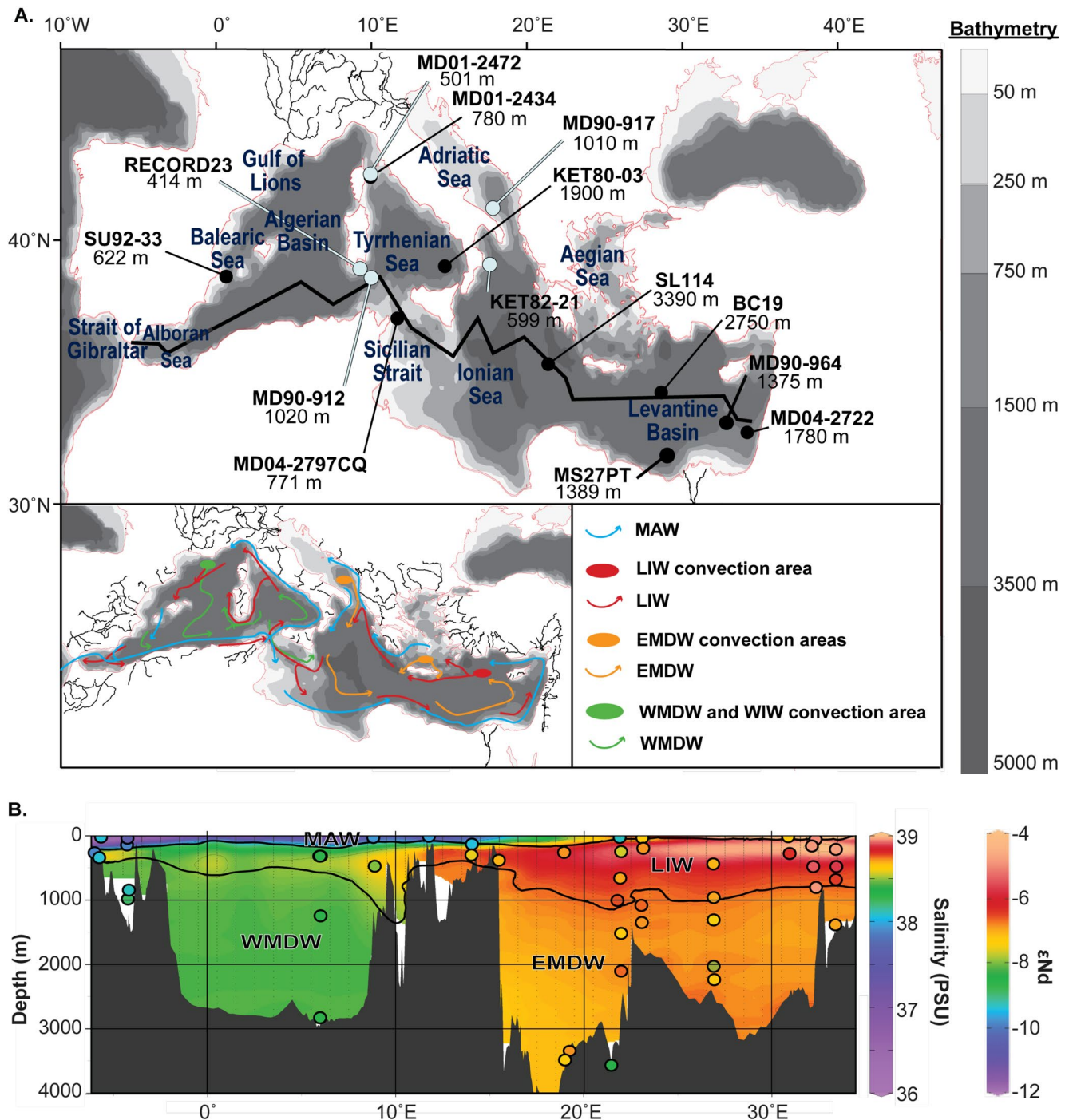


Figure 1. (a) Bathymetric map of the Mediterranean Sea showing locations of core MD01-2472 (42°36.42'N, 9°43.97'E; water depth 501 m), core RECORD23 (38°42.18'N, 8°54.75'E; water depth 414 m), core MD90-912 (38°18.67'N, 9°46.12'E, water depth 1020), core KET82-21 (38.99°N, 17.43°E; water depth 599 m), core MD90-917 (41°17'N, 17°37'E, 1,010 m) (blue dots) and all of the other sites discussed in this study (black dots). The simplified circulation of important water masses in the Mediterranean Sea is indicated in blue (MAW), red (LIW), yellow (EMDW) and green (WMDW) (b) Longitudinal transect of annual mean salinity of the Mediterranean Sea (i.e., the red shading shown in (a); data from WOA13). ϵNd values are represented by colored dots (Henry et al., 1994; Tachikawa et al., 2004; Vance et al., 2004). The map and section were generated using Ocean Data View software (Schlitzer, 2018). MAW: Modified Atlantic Water; LIW: Levantine Intermediate Water; EMDW: Eastern Mediterranean Deep Water; WMDW: Western Mediterranean Deep Water; WIW: Western Intermediate Water.

(Ionian Sea and Tyrrhenian Sea) as well as the Adriatic Sea, which is one of the main areas of deep-water formation of the EMS.

For the WMS, core MD01-2472 (42°36.42'N, 9°43.97'E; water depth 501 m; Toucanne et al., 2012) was collected in 2001 on the upper continental slope of the eastern part of the Corsica Trough during MD124-Geosciences cruise on board the R/V *Marion Dufresne* (Figure 1a). The lithology of core MD01-2472 consists of homogeneous brownish, muddy to silty sediments. The Corsica Trough is narrow (10–30 km at the 200 m isobath) and shallow (430–800 m) and connects the Ligurian and Tyrrhenian Seas through the northward flow of MAW above 200 m and LIW between 200 and 600–800 m (Astraldi & Gasparini, 2002; Millot, 1999, 2006). Core MD01-2472 is located within the modern core of the LIW flowing through the Corsica Trough.

Core RECORD23 (38°42.18'N, 8°54.75'E; water depth 414 m; Figure 1a) was collected in 2013 south of Sardinia during the cruise RECORD aboard the R/V *Urania* (Taviani et al., 2015). The lithology of core RECORD23 consists of brownish, muddy to silty, carbonate-rich sediments with intercalated levels of fragments of *Madrepora oculata* and *Lophelia pertusa* cold-water corals (Dubois-Dauphin et al., 2017). The present-day hydrographic structure of the Sardinia Channel is characterized by MAW, LIW, and TDW-WMDW (Astraldi, Conversano, et al., 2002; Millot & Taupier-Letage, 2005). In addition, the Western Intermediate Water (WIW), flowing between the MAW and the LIW, has also been observed along the Channel (Sammari et al., 1999). The core of the LIW is located at 400–450 m water depth in the Tyrrhenian Sea (Astraldi, Gasparini, et al., 2002; Hopkins, 1988), corresponding with the core depth of RECORD23 (414 m depth) from the Sardinia Channel (Taviani et al., 2015). The comparison of the ϵNd records obtained from cores MD01-2472 and RECORD23 enables us to compare the Holocene evolution of ϵNd in both branches of the LIW in the Tyrrhenian Sea (Figure 1a).

Core MD90-912 (38°18.67'N, 9°46.12'E, water depth 1,020 m; Figure 1a) was collected in 1990 at a location to the south of Sardinia during the PROMETE Leg I campaign aboard the R/V *Marion Dufresne*. The core site is in deeper water to the south east of core RECORD23 and is located in the modern TDW. It consists of a homogeneous brownish, muddy, carbonate-rich sediment.

For the EMS, core KET82-21 (38.99°N, 17.43°E; water depth 599 m; Figure 1a) was collected in 1982 in the north western Ionian Sea during the R/V *Le Suroît* cruise ETNA. The lithology of core KET82-21 consists of a fairly uniform succession of gray to brown carbonaceous clays, including a black layer in the upper part of the core and several ash layers. Core KET82-21 is located within the westward path of the LIW after it has partially recirculated in the Adriatic Sea (Millot & Taupier-Letage, 2005). Core MD90-917 (41°17'N, 17°37'E, 1,010 m; Figure 1a) was collected in 1990 in the south Adriatic Basin during the PROMETE Leg II cruise aboard the R/V *Marion Dufresne*. Coring at this site recovered a fairly uniform succession of gray to brown carbonaceous clays, including a black layer in the upper part of the core that refers to the two sub-units of the sapropel S1 and several ash layers (Siani et al., 2004). This core is located in the upper AdDW which results from the winter mixing of surface water (mainly MAW) and LIW.

3. Methods

3.1. Radiocarbon Dating

Radiocarbon dating was undertaken at the UMS-ARTEMIS Facility (CNRS-CEA Saclay, France) using a Pelletron 3 MV AMS on 8 mg of well-preserved calcareous test samples of planktonic foraminifera (mono-specific samples of *Globigerinoides ruber*, *Globigerina bulloides*, and *Globigerina inflata* and a mix of planktonic foraminifera for one sample) in the size fraction $>150\ \mu\text{m}$ (Table 1). The age models for the cores were derived from the calibrated planktonic ages by applying a variable sea-surface reservoir ^{14}C correction (Siani et al., 2000, 2001) and using INTCAL20 (Reimer et al., 2020) calibration curve in the Oxcal 4.4 software (Bronk Ramsey, 2009).

3.2. Stable Isotopes

Stable oxygen isotope measurements were performed on cores RECORD23, MD90-912 and KET82-21, on 10–20 hand-picked and well-preserved (clean and intact) specimens of the planktonic foraminifera *G.*

Table 1
AMS ^{14}C Ages of Samples of the Planktonic Foraminifera From Sediment Cores KET82-21, MD90-912, and RECORD23

Core	Depth (cm)	Species	^{14}C age (yr BP $\pm 1\sigma$)	Calendar age (cal. yr BP $\pm 1\sigma$)
KET82-21	0	<i>G. ruber</i> & <i>G. inflata</i>	1,705 \pm 30	1,230 \pm 50
KET82-21	89	<i>G. ruber</i>	7,970 \pm 35	8,380 \pm 20
KET82-21	115	<i>G. bulloides</i>	13,760 \pm 60	16,080 \pm 100
KET82-21	199	<i>G. bulloides</i>	25,830 \pm 200	29,650 \pm 315
KET82-21	250	<i>G. bulloides</i>	29,030 \pm 290	32,940 \pm 550
MD90-912	2	<i>G. inflata</i>	3,895 \pm 30	3,770 \pm 55
MD90-912	25	<i>G. inflata</i>	10,710 \pm 40	12,090 \pm 240
MD90-912	39	<i>G. inflata</i>	14,780 \pm 60	17,520 \pm 160
MD90-912	125	<i>G. inflata</i>	34,810 \pm 580	39,630 \pm 680
RECORD23	13	<i>G. inflata</i>	225 \pm 30	0 \pm 30
RECORD23	79	<i>G. inflata</i>	2,965 \pm 30	2720 \pm 60
RECORD23	114*	<i>G. inflata</i>	5,525 \pm 30	5,830 \pm 80
RECORD23	192*	<i>G. inflata</i>	8,190 \pm 35	8,560 \pm 40

Note. The AMS ^{14}C ages were corrected for ^{13}C and were converted to calendar years (cal. yr BP, BP = 1950 CE) using INTCAL20 (Reimer et al., 2020) calibration curve in the Oxcal 4.4 software (Bronk Ramsey, 2009) and assuming a mean constant surface ocean reservoir age of ~ 400 years for the Mediterranean Sea (Siani et al., 2000, 2001).

bulloides (fraction 250–315 μm). Samples were analyzed at the State Key Laboratory of Marine Geology (Tongji University) using a Finnigan MAT-253 mass spectrometer (Cheng et al., 2005). Shell oxygen isotope values are expressed in conventional delta notation (δ) relative to the isotopic ratio of the carbon dioxide gas derived from the Vienna Pee Dee Belemnite (VPDB) standard. Ratios are reported in ‰. VPDB is defined with respect to the NBS 19 ($\delta^{18}\text{O}$ of -2.20‰ VPDB), limestone standard. The mean external reproducibility was checked by replicate analyses of laboratory standards and is better than $\pm 0.14\text{‰}$ ($\pm 2\sigma$) for $\delta^{18}\text{O}$.

3.3. Neodymium Isotope Analyses

Neodymium isotopes were measured on 15–30 mg mixed planktonic foraminifera from the washed $>150\ \mu\text{m}$ size fraction of the samples without any oxidative-reductive leaching procedure, as this approach was demonstrated to be suitable for extracting deep-water Nd isotopic compositions (e.g., Tachikawa et al., 2014; Wu et al., 2015). Cleaning procedure and purification of Nd have been done in a class 100 clean laboratory using ultrapure reagents. The foraminifera tests were crushed between two glass slides to open chambers. The calcite fragments were then ultrasonicated for 1 min in MilliQ water before pipetting out the suspended particles. This step was repeated until the water was clear and free of clay particles. Samples were inspected under a binocular microscope to ensure that all sediment particles were removed, before they underwent a weak acid leaching for 5 min in 1 ml 0.001 M HNO_3 with ultrasonication. After the cleaning step, samples were transferred into a 1.5 ml tube, soaked in 0.5 ml MilliQ water and dissolved using stepwise 100 μl 0.5 M HNO_3 until the dissolution reaction stopped. The dissolved samples were centrifuged, and the supernatant was immediately transferred to Teflon beakers to prevent the leaching of any possible remaining phases. The solutions were then dried using a hotplate for Nd purification (Wu et al., 2015).

Neodymium was purified using Eichrom TRU-Spec and Ln-Spec resins, following the analytical procedure described in Copard et al. (2010). The $^{143}\text{Nd}/^{144}\text{Nd}$ ratios were measured using the ThermoScientific Neptune^{plus} Multi-Collector Inductively Coupled Plasma Mass Spectrometer (MC-ICP-MS), hosted at LSCE. For the Nd isotope analyses, sample and standard concentrations were matched at 10 ppb. Mass-dependent fractionation was corrected by normalizing $^{146}\text{Nd}/^{144}\text{Nd}$ to 0.7219 (O’Nions et al., 1977) and applying an exponential fractionation law. During the analytical sessions, every set of two samples was bracketed by anal-

yses of the La Jolla Nd standard solution, which is characterized by certified values of 0.511858 ± 0.000007 (Lugmair et al., 1983). The offset value between the results and the certified values of La Jolla was less than 0.4 epsilon units for all of the analyses presented in this study. The analytical errors reported herein correspond to the external two-sigma standard deviation (based on repeated analyses of the La Jolla standard for the different analytical sessions). The obtained analytical errors ranged from 0.1 to 0.6 epsilon units. The analytical blank values for Nd obtained for the full procedure were <4 pg, which represents less than 0.1% of the minimum Nd yield from foraminifera (around 4 ng) used in this study. As a result, no blank correction was applied.

4. Results

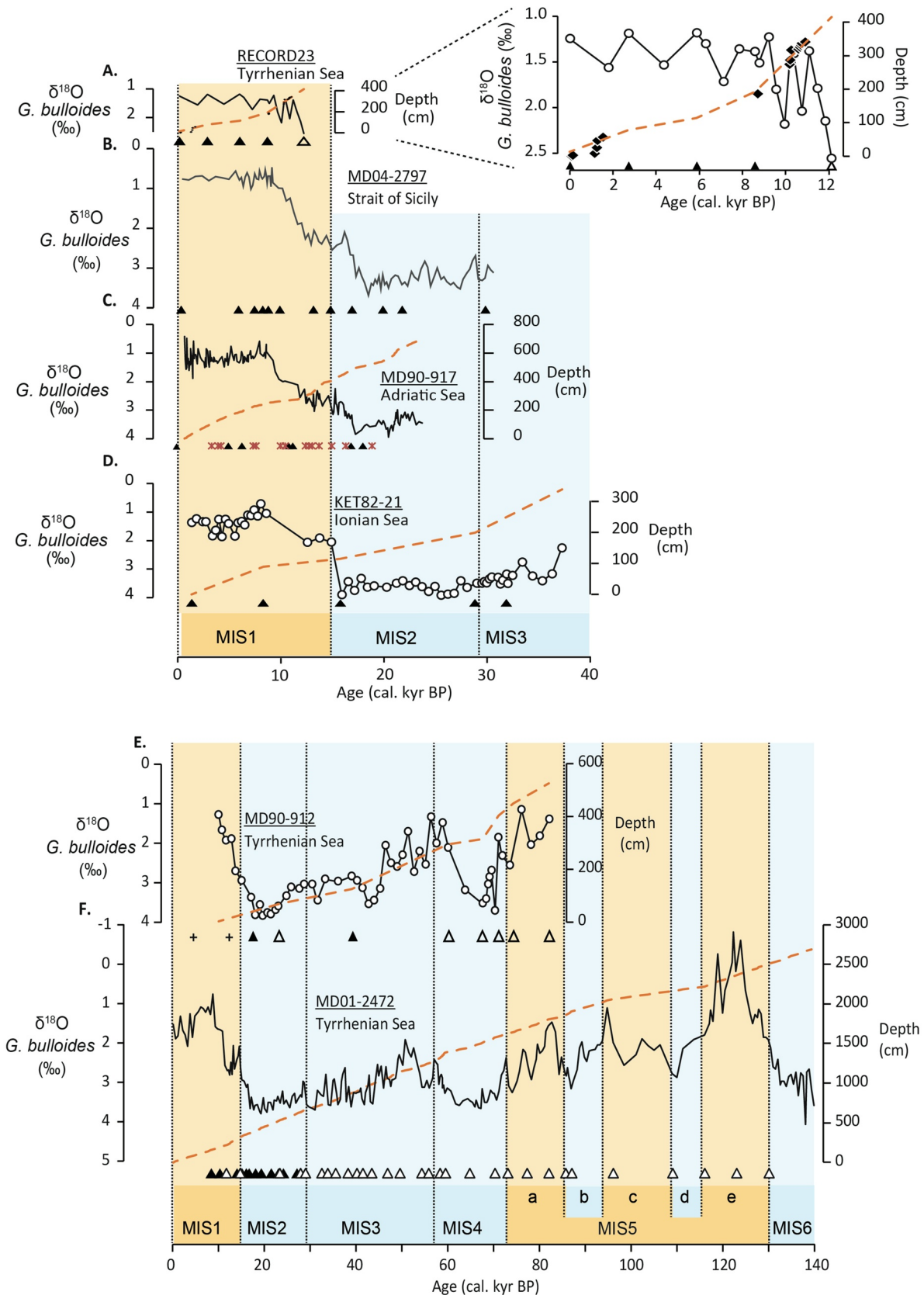
4.1. Chronological Framework

The chronologies of the studied cores were based both on the $\delta^{18}\text{O}$ stratigraphy of the planktonic foraminifera *G. bulloides* and on the radiocarbon ages obtained from planktonic foraminifera samples. For cores MD90-917, MD04-2797, and MD01-2472, the age models were previously published in Siani et al. (2010), Toucanne et al. (2012), and Cornuault et al. (2018), respectively Figures (2b–2c and 2f).

The oxygen isotope record of *G. bulloides* from the upper 415 cm of core RECORD23 is displayed in Figure 2a. The $\delta^{18}\text{O}$ record indicates that values remain largely invariable at $\sim 1.5\text{‰}$ for the upper 350 cm, similar to the Holocene $\delta^{18}\text{O}$ values from the well-dated neighboring Strait of Sicily core MD04-2797 (Figure 2b) (Essallami et al., 2007; Sicre et al., 2013) and the Tyrrhenian core MD01-2472 (Figure 2f) (Toucanne et al., 2012). By contrast, slightly higher $\delta^{18}\text{O}$ values are observed between 350 and 415 cm which are related to the Younger Dryas/Holocene transition (Figure 2a). Four calibrated AMS ^{14}C dates obtained on *G. inflata* have permitted us to establish an age model indicating that the upper 415 cm cover the last 12 cal kyr BP (Table 1; Figure 2a). In Figure 2a, we have also reported the U/Th ages of cold-water corals investigated on this core by Dubois-Dauphin et al. (2017). Cold-water coral U/Th ages range from 0.09 ± 0.01 to 10.90 ± 0.04 kyr BP and are distributed over three distinct periods of sustained coral occurrence: (i) between ~ 10.9 and 10.2 kyr BP, (ii) the Early Holocene at ~ 8.7 kyr BP and (iii) the Late Holocene starting at ~ 1.5 kyr BP (Figure 2a) (Dubois-Dauphin et al., 2017). Cold-water coral U/Th ages reported in Figure 2a are consistent with interpolation between foraminifer ^{14}C dates and tie-points attributed at the bottom of the core from the *G. bulloides* $\delta^{18}\text{O}$ record. This confirms the robustness of our age model for this core. The mean sedimentation rate of core RECORD23 is high (31 cm/kyr) (Figure 2a), allowing us to obtain a high temporal resolution of foraminiferal ϵNd during the Holocene.

For core KET82-21, the *G. bulloides* $\delta^{18}\text{O}$ record displays a glacial to Holocene $\delta^{18}\text{O}$ difference (considering maximum and minimum values) of $\sim 2.5\text{‰}$ in the upper 350 cm of the core (Figure 2d). Linear interpolation between five calibrated AMS ^{14}C dates obtained from planktonic foraminifera (>150 μm) was used to establish an age model for the upper 250 cm and linear extrapolation was applied for the part below 250 cm depth (Table 1; Figure 2d). The core KET82-21 covers the last ~ 38 ka with a mean sedimentation rate of 7.5 cm/ka.

The age model of core MD90-912 has been established using linear interpolation from four calibrated AMS ^{14}C dates obtained on planktonic foraminifer *G. inflata* (Table 1; Figure 2e) for the upper 125 cm. Below 125 cm depth, we correlated the *G. bulloides* $\delta^{18}\text{O}$ record to that of the nearby well dated core MD01-2472 (Figure 2f) (Toucanne et al., 2012). *G. bulloides* $\delta^{18}\text{O}$ of core MD90-912 varies from 1.3 to 3.8‰ over the last 82 kyr (Figure 2e). The age of the core-top (3.8 cal kyr BP) and the $\delta^{18}\text{O}$ record indicate that the top 20 cm of the core are perturbed, presumably as a result of the applied coring technique. Consequently, we did not investigate foraminiferal ϵNd for this depth interval. Below this, the AMS ^{14}C date obtained at 45 cm gives an age of 18.0 cal kyr BP in agreement with $\delta^{18}\text{O}$ values characteristic of the late glacial period (3.8‰) (Figure 2e). According to previous records from the Tyrrhenian Sea and the WMS (Martrat et al., 2004; Paterne et al., 1999; Toucanne et al., 2012), the lower *G. bulloides* $\delta^{18}\text{O}$ between 175 and 305 cm (reaching up to 1.3‰) is attributed to the early MIS3, whereas the higher $\delta^{18}\text{O}$ values between 275 and 405 cm are indicative of the MIS4 (Figure 2e). The mean sedimentation rate of core MD90-912 is 7.3 cm/kyr.



4.2. Nd Isotopic Composition of Planktonic Foraminifera

In the WMS, core MD01-2472, located at 501 m in the Corsica Trough (Figure 1a), displays ϵNd values ranging from -8.5 ± 0.2 to -7.2 ± 0.2 for the last climatic cycle (last 135 cal kyr BP) (Table 2; Figures 3e and 4). Unfortunately, the time interval between 110 and 90 cal kyr BP includes only one foraminiferal ϵNd value as the number of planktonic foraminifera was not sufficient to measure Nd isotopes. In general, long-term variations of foraminiferal ϵNd of core MD01-2472 (Figure 3e) covariate with the solar insolation at 20°N in summer (June) (Figure 3b). Each maximum of the insolation curve corresponds to a slight increase in ϵNd value observed at 125-121 cal kyr BP, 101 cal kyr BP, 85-79 cal kyr BP, 54-47 cal kyr BP, 31-26 cal kyr BP, and 13-6 cal kyr BP, respectively. ϵNd values are then higher during the early Holocene and the warm interstadials MIS5a, MIS5c, and MIS5e. In contrast, cold stadial MIS5b, MIS5d as well as the glacial MIS6 and MIS4 to MIS2 are characterized by slightly lower ϵNd values. Superimposed on these precessional long-term changes, the last glacial period is characterized by several millennial peaks of more radiogenic ϵNd (reaching up to -7.4 ± 0.2) at 46, 38, 28, and 17 cal kyr BP (Figure 3e). According to the chronological framework reported in Toucanne et al. (2012) for core MD01-2472, these slight ϵNd increases are coeval with increased iceberg discharges in the North Atlantic corresponding to the Heinrich Stadials HS5, HS4, HS3, and HS1 (Figure 3). The YD time interval (from 12.8 to 11.5 cal kyr BP) is also associated with radiogenic ϵNd values at intermediate depth in the Corsica Trough (Figure 3e). In addition, ϵNd increases to more radiogenic values (up to -7.2 ± 0.2) in the time interval between 14.1 and 6.2 cal kyr BP (Figures 3e and 4). Two ϵNd maxima are recorded at 9.3 and 6.5 cal kyr BP. This radiogenic time interval is interrupted at 8.2 cal kyr BP by a short interval associated with a more unradiogenic value (-7.8 ± 0.2). The ϵNd then decreases to lower values (-8.2 ± 0.3) after 6.5 cal kyr BP.

Core MD90-912, located south of Sardinia at 1,020 m water depth (Figure 1a), enables us to reconstruct past ϵNd of the TDW for the time interval between 69 and 21 cal kyr BP. Foraminiferal ϵNd ranges from -8.8 ± 0.2 to -6.8 ± 0.4 (Table 2; Figure 3d). The time interval between 52 and 58 cal kyr BP, corresponding to a maximum of summer insolation, is also associated with more radiogenic ϵNd values (up to -6.8 ± 0.4).

Core RECORD23, located at 414 m in the Sardinia Channel (Figure 1a), displays a range of ϵNd values that are slightly more radiogenic than those of core MD01-2472, varying from -8.9 ± 0.2 to -6.4 ± 0.2 for the last 12 cal kyr BP (Table 2; Figure 4). The highest ϵNd values (between -7.0 ± 0.2 and -6.4 ± 0.2) occur between 9.2 and 6 cal kyr BP, with a short interval from 8.6 to 7.9 cal kyr BP exhibiting unradiogenic values (reaching -7.7 ± 0.2). The Late Holocene (after 6 cal kyr BP) is marked by a continuous decrease of the ϵNd values which reach -8.9 ± 0.2 at 1.5 cal kyr BP (the most unradiogenic value) and -8.0 ± 0.4 at the core-top (Figure 4).

The Nd isotopic composition of core MD90-917, collected in the Adriatic Sea (Figure 1a), varies within a narrow range, from -6.4 ± 0.2 to -5.6 ± 0.4 , with an average value of -6.1 ± 0.2 ($n = 17$; 1σ) (Table 2, Figure 4). The ϵNd record shows slightly less radiogenic Nd isotopic compositions from 20 to 13.5 cal kyr BP and a modest increase toward the Holocene (Figure 4). The foraminiferal ϵNd record obtained from site KET82-21, located in the core of the intermediate water (599 m water depth, Figure 1) of the north-western Ionian Sea, also displays a narrow range of ϵNd (from -7.0 ± 0.2 to -6.4 ± 0.1) for the time interval between 19.4 and 7.8 cal kyr BP (Table 2; Figure 4).

Figure 2. Age models of cores RECORD23, MD04-2797, MD90-917, KET82-21, MD90-912, and MD01-2472, based on planktonic foraminifer oxygen isotopes ($\delta^{18}\text{O}$) and absolute dating data (i.e., ^{14}C and U/Th dates). The depth-age curves (dashed orange line) for different cores are shown, along with the Marine Isotope Stages (MIS). Radiocarbon dates are reported by filled triangles and isotope event tie points by open triangles (a) Planktonic foraminifer (*G. bulloides*) $\delta^{18}\text{O}$ (black line and white circles, ‰ vs. V-PDB) for core RECORD23, isotope event tie point (open triangle) has been obtained by correlation with *G. bulloides* $\delta^{18}\text{O}$ obtained on core MD04-2797 (Essallami et al., 2007; Sicre et al., 2013), cold-water coral depth and U/Th dates (black diamonds on zoom-in graph, Dubois-Dauphin et al., 2017); (b) *G. bulloides* $\delta^{18}\text{O}$ (‰ vs. V-PDB) on core MD04-2797 (Essallami et al., 2007; Sicre et al., 2013); (c) *G. bulloides* $\delta^{18}\text{O}$ (‰ vs. V-PDB) on core MD90-917 (Siani et al., 2010); (d) *G. bulloides* $\delta^{18}\text{O}$ (white circles, ‰ vs. V-PDB) on core KET82-21; (e) *G. bulloides* $\delta^{18}\text{O}$ (white circles, ‰ vs. V-PDB) on core MD90-912, radiocarbon dates (filled triangles), discarded radiocarbon dates (crosses). Isotope event tie points (open triangles) have been obtained by correlation with *G. bulloides* $\delta^{18}\text{O}$ obtained on core MD01-2472 (Toucanne et al., 2012); (f) *G. bulloides* $\delta^{18}\text{O}$ (black line, ‰ vs. V-PDB) on core MD01-2472, radiocarbon dates (filled triangles) (Toucanne et al., 2012). The MIS boundaries in this figure as well as in other figures in this study have been determined following Lisiecki and Raymo (2005).

Table 2

Nd Isotope Composition Obtained on Mixed Planktonic Foraminifera Samples From Cores MD01-2472, KET82-21, MD90-912, RECORD23, and MD90-917

Depth (cm)	Age (kyr BP)	$^{143}\text{Nd}/^{144}\text{Nd}$	$\pm 2\sigma$	ϵNd	$\pm 2\sigma$
MD01-2472 (42°36.42'N, 9°43.97'E; water depth 501 m; length 29.1 m)					
40	2.2	0.512231	± 0.000011	-7.9	± 0.2
80	4.4	0.512217	± 0.000013	-8.2	± 0.3
110	6.0	0.512257	± 0.000012	-7.4	± 0.2
120	6.5	0.512263	± 0.000019	-7.3	± 0.4
130	7.1	0.512252	± 0.000010	-7.5	± 0.2
150	8.2	0.512238	± 0.000011	-7.8	± 0.2
170	9.3	0.512267	± 0.000012	-7.2	± 0.2
230	12.1	0.512264	± 0.000012	-7.3	± 0.2
270	13.3	0.512250	± 0.000017	-7.6	± 0.3
330	15.1	0.512234	± 0.000010	-7.9	± 0.2
340	15.5	0.512231	± 0.000015	-7.9	± 0.3
370	16.8	0.512257	± 0.000011	-7.4	± 0.2
400	18.0	0.512217	± 0.000010	-8.2	± 0.2
420	18.8	0.512228	± 0.000019	-8.0	± 0.4
440	19.7	0.512231	± 0.000009	-7.9	± 0.2
490	21.7	0.512222	± 0.000011	-8.1	± 0.2
540	23.8	0.512226	± 0.000008	-8.0	± 0.2
566	25.0	0.512201	± 0.000010	-8.5	± 0.2
590	26.0	0.512219	± 0.000008	-8.2	± 0.2
620	27.4	0.512229	± 0.000013	-8.0	± 0.3
660	28.8	0.512231	± 0.000011	-7.9	± 0.2
683	30.0	0.512228	± 0.000009	-8.0	± 0.2
699	31.0	0.512211	± 0.000015	-8.3	± 0.3
732	33.0	0.512228	± 0.000010	-8.0	± 0.2
799	35.7	0.512207	± 0.000013	-8.4	± 0.3
810	36.4	0.512207	± 0.000013	-8.4	± 0.3
830	37.2	0.512241	± 0.000015	-7.8	± 0.3
850	37.9	0.512225	± 0.000013	-8.1	± 0.3
870	38.8	0.512247	± 0.000008	-7.6	± 0.2
893	40.0	0.512208	± 0.000010	-8.4	± 0.2
910	40.7	0.512212	± 0.000008	-8.3	± 0.2
940	41.7	0.512213	± 0.000015	-8.3	± 0.3
1020	45.0	0.512220	± 0.000010	-8.2	± 0.2
1030	45.5	0.512215	± 0.000013	-8.2	± 0.3
1050	46.4	0.512227	± 0.000010	-8.0	± 0.2
1070	47.2	0.512221	± 0.000015	-8.1	± 0.3
1100	48.2	0.512245	± 0.000011	-7.7	± 0.2
1156	50.5	0.512240	± 0.000010	-7.8	± 0.2
1181	52.1	0.512223	± 0.000009	-8.1	± 0.2

5. Discussion

5.1. Significance of Past ϵNd Variations Obtained on Foraminifera of Sediments From the Central Mediterranean Sea

Past seawater Nd isotopic compositions of water masses from the Mediterranean Sea have been reconstructed following various analytical procedures, many of which are still under debate within the scientific community. Nd isotopic compositions have been obtained from fish debris/teeth (Wu et al., 2019), planktonic foraminifera (Cornuault et al., 2018; Duhamel et al., 2020; Jiménez-Espejo et al., 2015; Osborne et al., 2010; Scrivner et al., 2004; Vance et al., 2004; Wu et al., 2019), cold-water corals (Dubois-Dauphin et al., 2017), and authigenic oxy-hydroxides using analytical procedures such as hydroxylamine hydrochloride of non-decarbonated samples (Cornuault et al., 2018; Tachikawa et al., 2004). All of these have been deemed suitable for extracting the ϵNd signature of oceanic deep-water masses but they may be affected by potential bias mainly due to contamination from lithogenic Nd of the detrital fraction (e.g., Wilson et al., 2013) or early diagenetic overprinting (e.g., Skinner et al., 2019).

Nevertheless, previous studies have demonstrated that ϵNd of uncleaned fossil planktonic foraminifera reflects bottom water ϵNd values due to the presence of authigenic Fe-Mn coatings precipitated onto the carbonate shells (e.g., Piotrowski et al., 2012; Roberts et al., 2012; Wu et al., 2015; Xu et al., 2018). This is supported by our new core top ϵNd data from the Tyrrhenian Sea. For core MD01-2472, the ϵNd value at the core-top (-7.9 ± 0.2 , Table 2) is similar to the modern ϵNd value of seawater from 400 to 600 m water depth at three water stations investigated in the northern Tyrrhenian Sea (mean $\epsilon\text{Nd} = -8.0 \pm 0.3$, $n = 4$; 2σ) (Garcia-Solsona & Jeandel, 2020). In addition, the core-top ϵNd value of core RECORD23 (-8.0 ± 0.4 , Table 2) is also similar to the closest modern seawater value at station RECORD28 (38°42.14'N–8°54.72'E, 451 m water depth, -8.0 ± 0.6).

It has been shown that eolian dust input can modify ϵNd distribution in the ocean (e.g., Stichel et al., 2015). Saharan dusts are characterized by unradiogenic ϵNd values (-15.4 to -11 ; Scheuven et al., 2013) and may thus contribute to the unradiogenic Nd signature of surface and intermediate water masses (e.g., Tachikawa et al., 2004). However, the present-day distribution of ϵNd in the surface and intermediate water masses of the Mediterranean Sea is mainly attributed to the mixing of the AW and the LIW and suggests a negligible contribution of lithogenic Nd input from eolian dusts (Tachikawa et al., 2004). This is mainly attributed to the relatively low Nd concentration and fractional solubility of eolian dusts (Tachikawa et al., 2004).

However, the last glacial period was associated with increased aridity in North Africa and higher fluxes of Saharan dust to the Mediterranean Sea (e.g., Ehrmann et al., 2017). In addition, Heinrich Stadial events are associated with increases in unradiogenic ϵNd dust inputs to the Mediterranean Sea (Ehrmann et al., 2017). These increases in dust inputs do not appear to have significantly modified the intermediate water ϵNd record obtained in core MD01-2472 since Heinrich Stadial events are systematically associated with more radiogenic ϵNd values (Figure 3). However, we cannot entirely exclude the possibility that a marked reduction in eo-

Table 2
Continued

Depth (cm)	Age (kyr BP)	$^{143}\text{Nd}/^{144}\text{Nd}$	$\pm 2\sigma$	ϵNd	$\pm 2\sigma$
1220	54.5	0.512234	± 0.000008	-7.9	± 0.2
1225	54.8	0.512216	± 0.000009	-8.2	± 0.2
1240	55.6	0.512220	± 0.000013	-8.2	± 0.2
1278	57.0	0.512220	± 0.000008	-8.2	± 0.2
1356	59.0	0.512224	± 0.000012	-8.1	± 0.2
1408	61.5	0.512222	± 0.000015	-8.1	± 0.3
1440	64.3	0.512210	± 0.000013	-8.3	± 0.3
1460	65.4	0.512214	± 0.000012	-8.3	± 0.2
1480	66.3	0.512229	± 0.000012	-8.0	± 0.2
1540	68.9	0.512225	± 0.000014	-8.1	± 0.3
1623	73.0	0.512212	± 0.000008	-8.3	± 0.2
1700	77.4	0.512224	± 0.000011	-8.1	± 0.2
1720	78.3	0.512206	± 0.000012	-8.4	± 0.2
1740	79.3	0.512259	± 0.000011	-7.4	± 0.2
1800	82.0	0.512240	± 0.000013	-7.8	± 0.2
1840	85.0	0.512234	± 0.000009	-7.9	± 0.2
1880	86.5	0.512206	± 0.000010	-8.4	± 0.2
2100	101.2	0.512262	± 0.000010	-7.3	± 0.2
2200	113.7	0.512214	± 0.000013	-8.3	± 0.3
2280	119.0	0.512224	± 0.000011	-8.1	± 0.2
2300	120.0	0.512226	± 0.000013	-8.0	± 0.2
2320	121.0	0.512244	± 0.000013	-7.7	± 0.2
2340	122.0	0.512246	± 0.000011	-7.6	± 0.2
2400	125.0	0.512241	± 0.000009	-7.7	± 0.2
2420	126.0	0.512215	± 0.000015	-8.3	± 0.3
2440	127.0	0.512210	± 0.000010	-8.3	± 0.2
2480	129.0	0.512229	± 0.000021	-8.0	± 0.4
2600	135.0	0.512221	± 0.000012	-8.1	± 0.2
KET82-21 (38.99°N, 17.43°E; water depth 599 m; length 11.11 m)					
82	7.8	0.512284	± 0.000011	-6.9	± 0.2
104	12.8	0.512302	± 0.000011	-6.6	± 0.2
116	16.2	0.512308	± 0.000007	-6.4	± 0.1
128	18.2	0.512279	± 0.000009	-7.0	± 0.2
136	19.4	0.512289	± 0.000008	-6.8	± 0.2
MD90-912 (38°18.67'N, 9°46.12'E; water depth 1020 m; length 16.33 m)					
55	20.7	0.512209	± 0.000008	-8.4	± 0.2
69	23.0	0.512219	± 0.000008	-8.2	± 0.2
115	36.1	0.512218	± 0.000011	-8.2	± 0.2
155	42.6	0.512227	± 0.000007	-8.0	± 0.1
185	46.4	0.512231	± 0.000013	-7.9	± 0.3
205	48.8	0.512230	± 0.000010	-8.0	± 0.2
225	51.3	0.512259	± 0.000013	-7.4	± 0.3

lian input during African Humid Periods (Bout-Roumazielles et al., 2013; Ehrmann et al., 2017) may have contributed to more radiogenic ϵNd in intermediate- and deep-water masses of the South Sardinian Channel and Corsica Trough. Nevertheless, it has been proposed elsewhere that Saharan dust had a negligible influence on the water masses of the Mediterranean Sea. ϵNd records obtained for the WMS (Dubois-Dauphin et al., 2017; Jiménez-Espejo et al., 2015) and the EMS (Cornuault et al., 2018; Wu et al., 2019) have indicated that glacial periods are not systematically associated with ϵNd values more unradiogenic than those of interglacial times (Figures 5b and 6) (Duhamel et al., 2020).

On the other hand, lithogenic Nd input from rivers can strongly influence the distribution of Nd in the oceans (e.g., Rousseau et al., 2015; Yu et al., 2018). For the Mediterranean Sea, it has been demonstrated that the Nile River (Tachikawa et al., 2004; Wu et al., 2019) and/or the process of “boundary exchange” between water masses and volcanic sediment along the eastern and northern margins of the Levantine Basin are major sources of lithogenic radiogenic Nd to the eastern Mediterranean Sea (Ayache et al., 2016). The dissolved ϵNd -values of water masses of the Mediterranean Sea have been demonstrated to be a two end-member mixing between volcanic radiogenic sediments (radiogenic Nile-derived material and Levantine margins sediment) in the east, and less radiogenic Atlantic waters inflowing from the west (Duhamel et al., 2020; Wu et al., 2019). This two end-member mixing is well illustrated in Figure 5 which plots the seawater ϵNd of the EMS and WMS versus longitude.

Past changes in bottom/pore water oxygen contents may induce preferential mobilization of Nd from solid phases (Wilson et al., 2013), with possible re-precipitation on fossil foraminifera samples from the pore water (Skinner et al., 2019). In the context of the Mediterranean Sea, and with respect to the large-scale anoxia or suboxia during sapropel deposition, lithogenic Nd could be then remobilized in the pore water sediments. However, sapropel depositions have not been observed in the Tyrrhenian Sea or at intermediate depth throughout the Mediterranean Sea. We can hypothesize, therefore, that bottom conditions at intermediate depth remain sufficiently oxygenated all of the time and that the mobilization of Nd from solid phases of cores MD01-2472 and RECORD23 can be considered to be negligible.

Taken together, these results suggest that changes in bottom/pore water oxygen contents or changes of eolian dust input since the last climatic cycle cannot explain the observed ϵNd variability at intermediate water depths in the central Mediterranean Sea.

5.2. Hydrological Settings of the Central Mediterranean Sea Over the Last 20 kyr

5.2.1. Neodymium Isotope Variations in the Intermediate Water Masses of the Tyrrhenian Sea

Modern hydrological observations have suggested a slightly higher contribution of LIW in the Sardinia Channel compared to the Corsica Trough (Hopkins, 1988). This is in close agreement with ϵNd records obtained in cores MD01-2472 (Corsica Trough) and RECORD23 (Sardinia Channel), with the latter displaying slightly higher values and a larger ampli-

Table 2
Continued

Depth (cm)	Age (kyr BP)	$^{143}\text{Nd}/^{144}\text{Nd}$	$\pm 2\sigma$	ϵNd	$\pm 2\sigma$
235	52.6	0.512232	± 0.000007	-7.9	± 0.1
255	55.0	0.512288	± 0.000018	-6.8	± 0.4
265	56.3	0.512225	± 0.000010	-8.1	± 0.2
265	56.3	0.512196	± 0.000010	-8.6	± 0.2
275	57.5	0.512239	± 0.000013	-7.8	± 0.2
285	58.8	0.512200	± 0.000010	-8.5	± 0.2
315	67.5	0.512188	± 0.000010	-8.8	± 0.2
345	68.7	0.512209	± 0.000011	-8.4	± 0.2
RECORD23 (38°42.18'N, 08°54.75'E; water depth 414 m; length 4.25 m)					
13	0.0	0.512230	± 0.000020	-8.0	± 0.4
49	1.5	0.512181	± 0.000012	-8.9	± 0.2
56	1.8	0.512253	± 0.000016	-7.5	± 0.3
79	2.7	0.512246	± 0.000017	-7.6	± 0.3
89	3.6	0.512252	± 0.000009	-7.5	± 0.2
97	4.3	0.512247	± 0.000018	-7.6	± 0.4
105	5.1	0.512265	± 0.000013	-7.3	± 0.2
114	5.9	0.512274	± 0.000015	-7.1	± 0.3
126	6.3	0.512265	± 0.000013	-7.3	± 0.2
134	6.6	0.512291	± 0.000011	-6.8	± 0.2
146	7.0	0.512281	± 0.000012	-7.0	± 0.2
163	7.6	0.512283	± 0.000013	-6.9	± 0.3
171	7.8	0.512309	± 0.000013	-6.4	± 0.2
173	7.9	0.512241	± 0.000012	-7.7	± 0.2
178	8.1	0.512272	± 0.000011	-7.1	± 0.2
192	8.6	0.512241	± 0.000021	-7.7	± 0.4
204	8.8	0.512252	± 0.000016	-7.5	± 0.3
218	9.0	0.512258	± 0.000017	-7.4	± 0.3
232	9.2	0.512304	± 0.000016	-6.5	± 0.3
243	9.4	0.512259	± 0.000011	-7.4	± 0.2
254	9.6	0.512236	± 0.000014	-7.8	± 0.3
293	10.2	0.512240	± 0.000013	-7.8	± 0.2
357	11.2	0.512257	± 0.000010	-7.4	± 0.2
407	12.0	0.512266	± 0.000010	-7.3	± 0.2
MD90-917 (41°17'N, 17°37'E; water depth 1010 m; length 21 m)					
18	0.9	0.512325	± 0.000018	-6.1	± 0.4
61	2.0	0.512333	± 0.000016	-6.0	± 0.3
100	3.1	0.512329	± 0.000011	-6.0	± 0.2
130	3.9	0.512328	± 0.000009	-6.1	± 0.2
179	5.6	0.512326	± 0.000012	-6.1	± 0.2
205	6.5	0.512314	± 0.000017	-6.3	± 0.3
235	7.9	0.512315	± 0.000019	-6.3	± 0.4
249	8.4	0.512331	± 0.000013	-6.0	± 0.3

tude of variations during the time interval of Sapropel 1 (S1) deposition (Figure 4).

The foraminiferal ϵNd record of core RECORD23 reported in Figure S1 integrates previous ϵNd values obtained from scleractinian cold-water corals (*Madrepora oculata* and *Lophelia pertusa*) from the same core (Dubois-Dauphin et al., 2017). Published cold-water coral ϵNd values exist for three time intervals during the Holocene and display a relatively larger range of ϵNd values, with values varying from -6.0 ± 0.5 to -7.7 ± 0.1 during the Early and Late Holocene and with values as low as -8.6 ± 0.3 at ~ 8.7 cal kyr BP (Figure S1). Overall, the ϵNd ranges obtained from both archives are quite similar (from -8.7 ± 0.3 to -6.0 ± 0.5 for the cold-water corals and from -8.9 ± 0.2 and -6.4 ± 0.2 for the foraminifera). Comparison between ϵNd records obtained on foraminifera and coral archives is complicated by the fact that only four of the foraminifera samples investigated here have a similar age (less than 300 years) to cold-water corals. The ϵNd of foraminifera samples at the core top (present time) and at 10.2 cal kyr BP are similar (within analytical 2σ error bars) to those of corals. ϵNd values of foraminifera samples at 1.5 and 8.8 cal kyr BP are different from those of corals which display a larger range of ϵNd values (up to 1–2 epsilon units) on a short time interval around age of these foraminifera samples. This larger range, reconstructed from cold-water corals, could be related to the rapid growth of corals and their ability to capture snapshots of seawater ϵNd integrated over a few years (Montero-Serrano et al., 2013), whereas ϵNd carried by Fe-Mn coatings on foraminifera was probably acquired over a much longer period of time at the seabed and are thus likely to integrate several hundreds to a few thousands of years of hydrological variations. Modern oceanographic observations in the Mediterranean Sea have shown decadal-scale hydrological variations. For example, in the late 1980s to early 1990s, the Aegean Sea produced denser water than the Adriatic Sea (Eastern Mediterranean Transient, Roether et al., 1996), due to enhanced Etesian winds over the Aegean Sea. The formation of this denser water had consequences further west on the TDW in the WMS (Schroeder et al., 2006). Such relatively short variations in water mass circulation are not recorded in the foraminifer coatings but may be preserved as a geochemical signal in coral skeletons. Thus, ϵNd analysis along a continuous branch of cold-water coral can be useful for evaluating such decadal variability of the ϵNd for the intermediate water of South of Sardinia and to explain the apparent discrepancy between the planktonic foraminifera and cold-water coral records.

The foraminiferal ϵNd records obtained from core RECORD23 show little variation (ϵNd of ~ -7.5) between 12 and 9.2 cal kyr BP, before a slight increase to -6.5 ± 0.3 at 9.2 cal kyr BP (Figure 4). Taking uncertainty in the age model into account, foraminiferal ϵNd obtained for the time interval of Sapropel S1 deposition in the EMS (10.2–6.4 cal kyr BP; De Lange et al., 2008; Mercone et al., 2000) indicates high values of up to -6.5 ± 0.3 at 9.2 and 7.8 cal kyr BP for core RECORD23. However, at 8.7 cal kyr BP, coral ϵNd drops to -8.7 ± 0.6 (Dubois-Dauphin et al., 2017) (Figure S1). Such ϵNd values have been confirmed by our foraminiferal record, which also displays unradiogenic values as low as -7.7 ± 0.4 between 8.6 and 8.0 cal kyr BP.

Table 2
Continued

Depth (cm)	Age (kyr BP)	$^{143}\text{Nd}/^{144}\text{Nd}$	$\pm 2\sigma$	ϵNd	$\pm 2\sigma$
260	9.6	0.512338	± 0.000019	-5.9	± 0.4
285	11.9	0.512325	± 0.000013	-6.1	± 0.2
310	12.6	0.512349	± 0.000022	-5.6	± 0.4
334	13.0	0.512325	± 0.000010	-6.1	± 0.2
365	13.5	0.512317	± 0.000012	-6.3	± 0.2
430	15.3	0.512315	± 0.000014	-6.3	± 0.3
460	16.1	0.512311	± 0.000012	-6.4	± 0.2
510	17.8	0.512316	± 0.000013	-6.3	± 0.3
550	19.8	0.512313	± 0.000011	-6.3	± 0.2

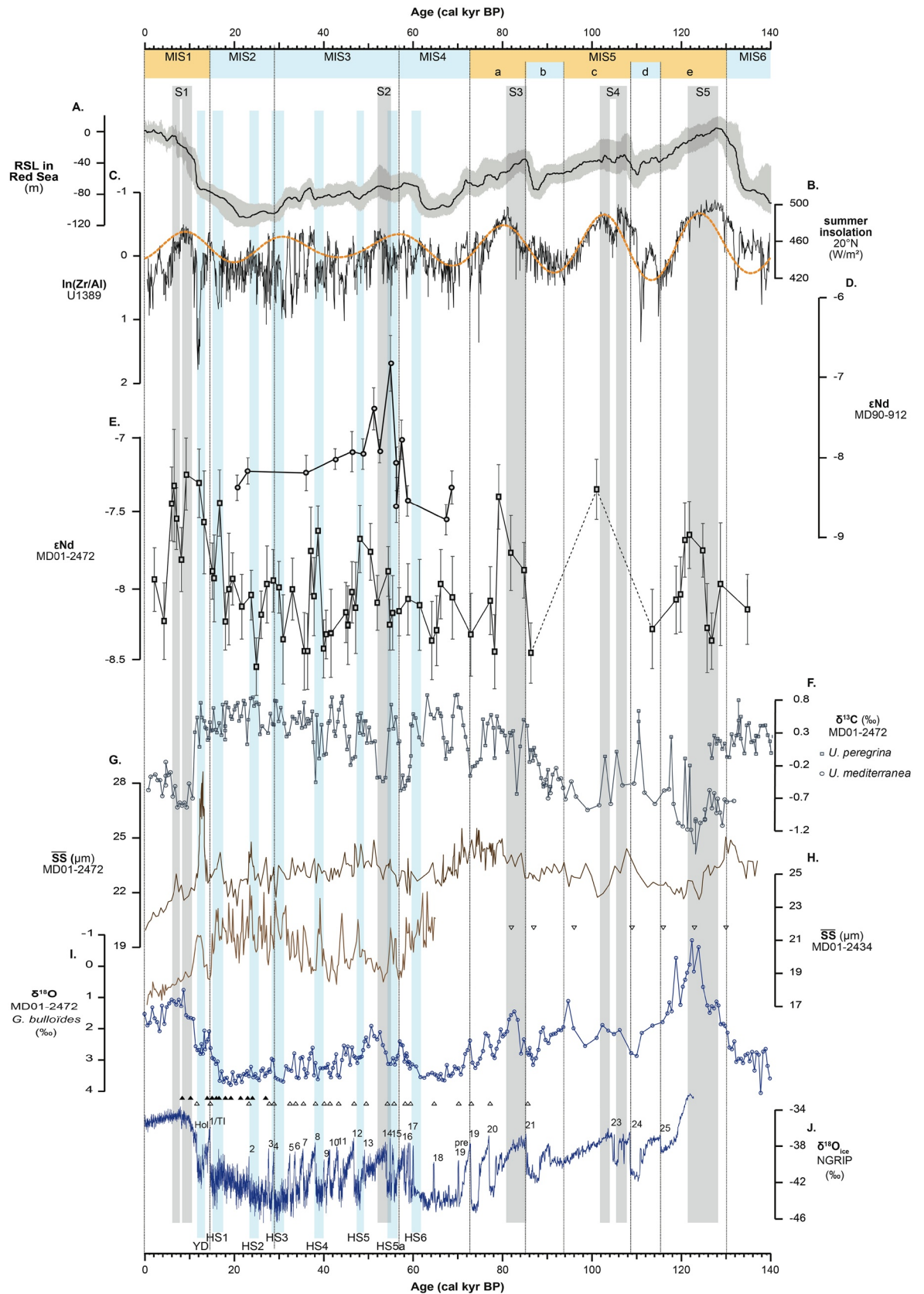
In the Corsica Trough, the foraminiferal ϵNd record of core MD01-2472 allows us to establish the Nd isotopic signature of the second branch of the LIW flowing in the Tyrrhenian Sea (Figure 1a). The ϵNd record of core MD01-2472 displays more radiogenic values (reaching -7.2 ± 0.2) between 14 and 6 cal kyr BP, coeval with the timing of the African Humid Period (AHP) (Bastian et al., 2017; Menot et al., 2020; Shanahan et al., 2015) (Figure 4). The time interval corresponding to the organic-rich sapropel S1a and S1b deposition in the EMS, i.e. between 10.2 and 6.4 cal kyr BP (De Lange et al., 2008; Mercone et al., 2000), is also associated with radiogenic ϵNd . However, one unradiogenic value (-7.8 ± 0.2) is recorded at 8.2 cal kyr BP (Figure 4). Taking into account age model uncertainty in both cores and particularly in core RECORD23, which is based on only four radiocarbon dates, this decrease in ϵNd in core MD01-2472 is likely to be coeval with the timing of low ϵNd observed in core RECORD23 between 8.6 and 7.9 cal kyr BP and may be attributed to the interruption of sapropel S1 deposition dated at 8.2 kyr in the EMS (e.g., Grant et al., 2012).

The good agreement observed in the long-term changes of the ϵNd in both branches of the LIW flowing in the western WMS during the Holocene suggests that cores RECORD23 and MD01-2472 provide a regional signal of the Nd isotopic composition of the intermediate water masses in the Tyrrhenian Sea (Figure 4). The time interval characterized by slightly higher ϵNd between 14 and 8.2 cal kyr BP is synchronous with the deposition of the ORL1 (14.5–8.2 cal kyr BP) in the Alboran Sea (WMS) (Cacho et al., 2002; Jimenez-Espejo et al., 2008; Rodrigo-Gamiz et al., 2011). This ORL was associated with less-ventilated deep waters in the WMS during the deglaciation, ending with a short interval of SST cooling during the 8.2 cal kyr BP cold event which has been observed in several marine and continental records for the Northern Hemisphere (Alley et al., 1997; Cacho et al., 2002; Rohling et al., 2015; Von Grafenstein et al., 1998). This cold event is also associated with a period of marked aridification in Northeast Africa (Costa et al., 2014; Garcin et al., 2012; Marshall et al., 2011) and re-ventilation of the deep-water and the interruption of the S1 deposition of the EMS (Filippidi et al., 2016; Rohling et al., 1997, 2002; Schmiedl et al., 2010; Siani et al., 2013; Tachikawa et al., 2015; Zirks et al., 2019). The time interval coeval with the deposition of the sapropel S1b in the EMS is not correlated to high TOC in the Alboran Sea (Rogerson et al., 2008) but displays similar high ϵNd in the Corsica Trough and Sardinia Channel than during the time interval of the deposition of the ORL1.

Nd isotopic composition at intermediate depth in the Corsica Trough and Sardinia Channel during the Holocene could be the result of changes in the ϵNd of the main water-mass end-members circulating at intermediate depth in the western Mediterranean basin (LIW and WIW) and/or of changes in the relative contribution of each water mass through time. Unfortunately, no information exists on the potential temporal variability in ϵNd of the water mass produced in the Gulf of Lions since the LGM. However, ϵNd records obtained at intermediate depth (core SU92-33; 622 m) in the Balearic Sea (Dubois-Dauphin et al., 2017) and at greater water depth (cores 302G and 304G; 1,989 and 2,382 m) in the Alboran Sea (Jiménez-Espejo et al., 2015) (Figure 7A) reveal a narrow range of variations. Accordingly, we hypothesize that the ϵNd of deep-water masses produced in the Gulf of Lions has not changed significantly since the last glacial period and remained relatively unradiogenic (e.g., ϵNd of -9.4 ± 0.9 for present-day WMDW; Henry et al., 1994; Tachikawa et al., 2004). This hypothesis needs to be verified by further investigation in the Gulf of Lions. Nevertheless, variations in the ϵNd of the WMDW alone cannot explain the ϵNd variations observed at intermediate depth in the Tyrrhenian Sea. Consequently, the time interval of radiogenic ϵNd observed in both records at intermediate depths between 14 and 6 cal kyr BP, and particularly during sapropel S1a and S1b deposition, is consistent with a higher contribution of LIW at the studied site and/or the same inflow of a LIW characterized by more radiogenic Nd isotopic signature during this time interval.

5.2.2. Comparison of the LIW ϵNd Between the Levantine Basin and the Tyrrhenian Sea

The ϵNd of the LIW flowing in the Tyrrhenian Sea has been recorded in the western part of the Strait of Sicily (core MD04-2797CQ; 771 m water depth) for the last 19 cal kyr BP (Cornuault et al., 2018) (Figure 7C). ϵNd values of the Strait of Sicily vary between -6.5 ± 0.2 and -2.5 ± 0.2 and are therefore higher than those



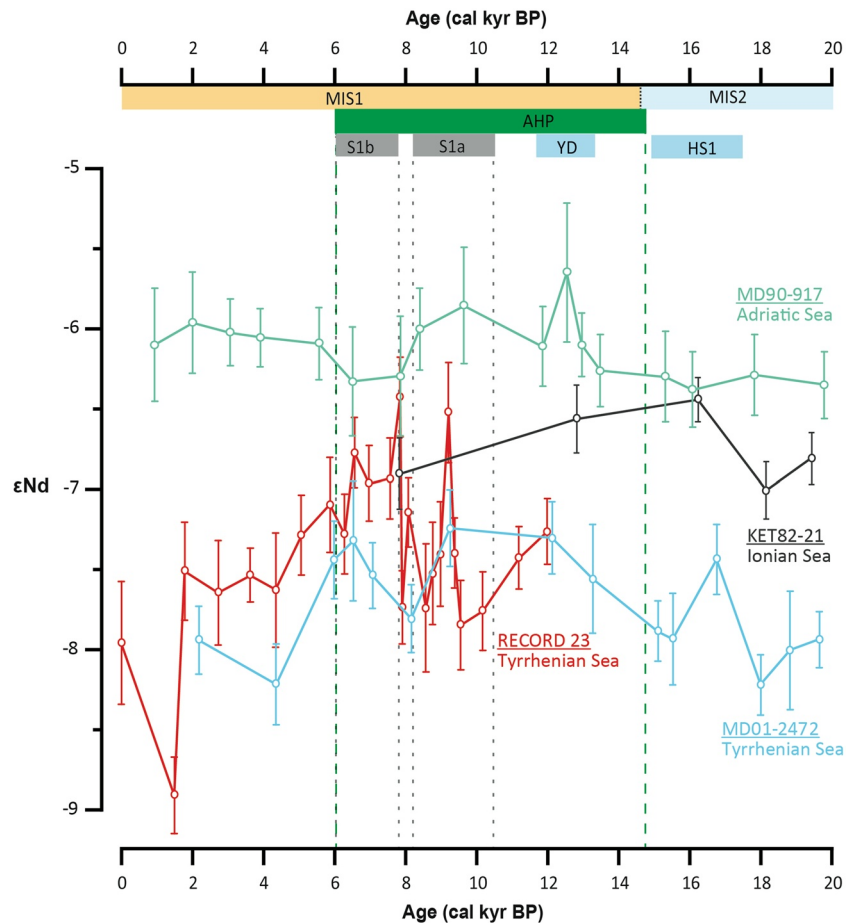


Figure 4. ϵ Nd obtained on non-reductively cleaned mixed planktonic foraminifera of core MD90-917, KET82-21, RECORD23 and MD01-2472 for the last 20 cal kyr BP. Also reported are Marine Isotope Stages (MIS), S1a and S1b as defined in Grant et al. (2016), YD and HS1 as defined in Toucanne et al. (2012), AHP as defined in Revel et al. (2010).

obtained from core KET82-21 located at intermediate depth in the north-western Ionian Sea (Figure 7B) and are not plotted on the west-east increasing trend observed in all the other intermediate cores of the Mediterranean Sea (Figure 5). Further investigations will be necessary to understand such large range of ϵ Nd variations obtained on core MD04-2797CQ. Nevertheless, core MD04-2797CQ presents similar long term variations of ϵ Nd values to those obtained from records in the eastern Levantine Basin, such as cores BC19, SL114, MD90-964, and MS27PT (Figures 7D and 7E) (Cornuault et al., 2018; Duhamel et al., 2020; Wu et al., 2019). All of these cores, collected in the upper EMDW/lower LIW, indicate more radiogenic values between 14 and 6 cal kyr BP, reaching up to -2.1 ± 0.2 for core MS27PT and -3.2 ± 0.2 for core MD90-964. After 6 cal kyr BP, ϵ Nd gradually decreases until 2 cal kyr BP in several cores from the EMS (MD04-2797CQ, MS27PT, MD04-2472). Such long-term ϵ Nd changes since the LGM, with more radiogenic values between 14 and 6 cal kyr BP and a steady decrease after 6 cal kyr BP, are also observed in cores RECORD23 and MD01-2472 with a lower ϵ Nd amplitude (Figures 4 and 7b). In addition, the ϵ Nd record obtained in

Figure 3. Comparison of paleoceanographic records over the last climatic cycle (since 140 cal kyr BP): (a) variations in the Relative Sea Level (RSL) (Grant et al., 2014); (b) summer insolation (June and July) received by the Earth at 20°N (Laskar et al., 2004), calculated using Analyseries software (Paillard et al., 1996); (c) variations of $\ln(\text{Zr}/\text{Al})$ from IODP Site U1389 (Bahr et al., 2015); (d) ϵ Nd obtained on mixed planktonic foraminifera from core MD90-912; (e) ϵ Nd values obtained on mixed planktonic foraminifera from core MD01-2472; (f) Benthic foraminifer (*U. peregrina* and *U. mediterranea*) $\delta^{13}\text{C}$ (‰ vs. V-PDB) for core MD01-2472 (Toucanne et al., 2012); (g) mean sortable silt size (μm) for core MD01-2472 (Toucanne et al., 2012); (h) mean sortable silt size (μm) for core MD01-2434 (Toucanne et al., 2012); (i) Planktonic foraminifer (*G. bulloides*) $\delta^{18}\text{O}$ (‰ vs. V-PDB) for core MD01-2472 (Toucanne et al., 2012); (j) Ice $\delta^{18}\text{O}$ (‰ vs. V-SMOW), GICC05 to 60 kyr (NGRIP dating group, 2008), NGRIP thereafter (NGRIP members, 2004). TI and TII are the Termination I and II, 2–25 are the Greenland Interstadials 2–25, YD is the Younger Dryas, HS1-HS6 are Heinrich Stadial events 1 to 6. Marine Isotope Stages (MIS) are also reported. S1 to S5 are Sapropel Events 1 to 5 in the Eastern Mediterranean (Grant et al., 2012).

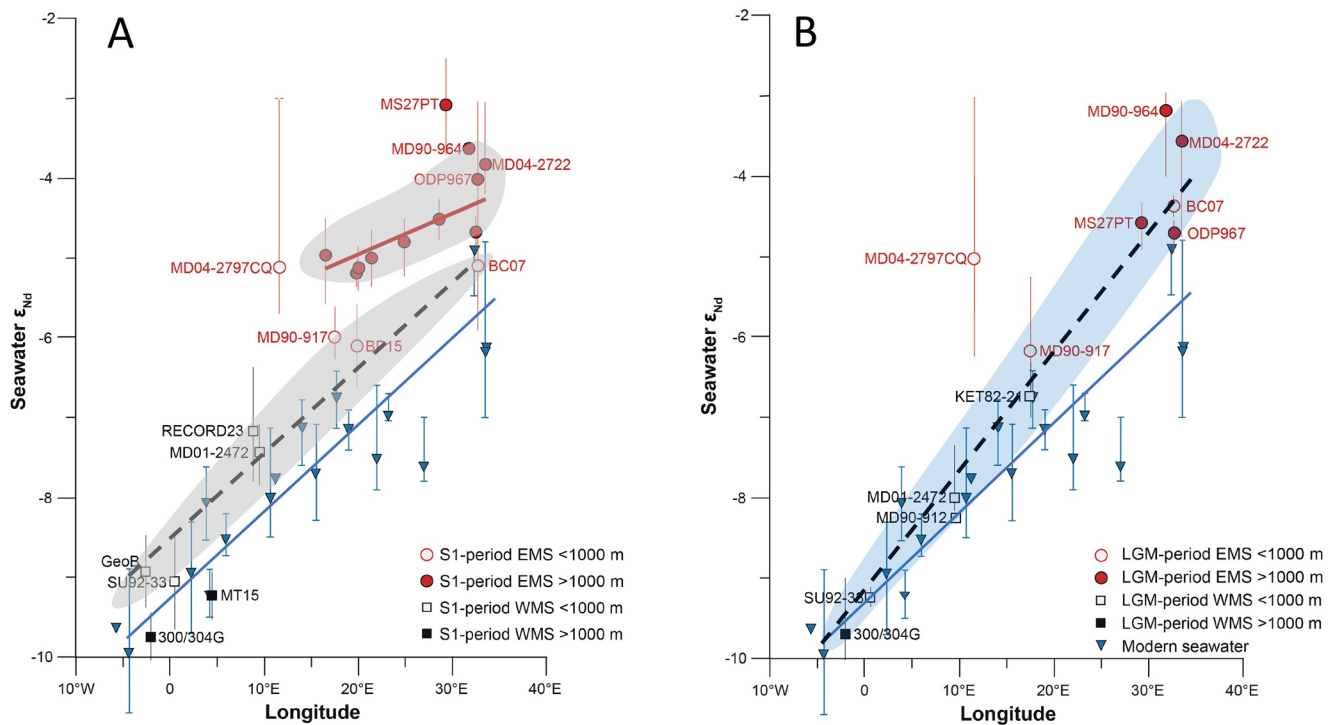


Figure 5. Average seawater- ϵ_{Nd} values versus longitude for the seawater, for the time interval of Sapropel 1 (S1) deposition (a) and for the Last Glacial Maximum (LGM) (b). Foraminiferal ϵ_{Nd} data are distinguished between the EMS (red circles, Cornuault et al., 2018; Duhamel et al., 2020; Freydl et al., 2001; Scrivner et al., 2004; Wu et al., 2019) and the WMS (black squares, Dubois-Dauphin et al., 2017; Jiménez-Espejo et al., 2015, this study). Open and solid symbols have been used to distinguish between data obtained on cores above and below 1,000 m depth, respectively). Blue triangles and trend-line indicate a progressive west-east increase in dissolved ϵ_{Nd} of modern seawater; blue error-bars depict the ϵ_{Nd} ranges of >200 m water-column (García-Solsona & Jeandel, 2020; Henry et al., 1994; Tachikawa et al., 2004; Vance et al., 2004). The different symbols represent average values and vertical bars depict the ϵ_{Nd} ranges.

the EMS (Duhamel et al., 2020; Wu et al., 2019), and notably in the Levantine Sea at greater depth, displays higher ϵ_{Nd} during S1a and even beforehand (14 cal kyr BP in the Levantine Basin) (Figures 7d and 7e). These ϵ_{Nd} records also display a significant decrease during the time interval of S1 deposition (Figures 7d and 7e), whereas in the Central Mediterranean Sea, ϵ_{Nd} is similarly high during S1a and S1b (Corsica Trough and South of Sardinia).

Nevertheless, the time interval coeval with the AHP is also associated with weaker current velocity and less oxygenated water masses as established by using sortable silt parameter and faunistic assemblage at site MD01-2472 (Angue Minto'o et al., 2015; Toucanne et al., 2012) (Figures 3g and 3h). Such variations, which start around 14 cal kyr BP, may be associated with an inflow of LIW characterized by a more radiogenic Nd isotopic signature. This is in agreement with Nile sediment discharge records that indicate an increasing discharge at ~15 cal kyr BP in core MS27PT which could have induced a freshening of the Mediterranean Sea and thus a more sluggish circulation (Revel et al., 2010). An estimation of the impact of sluggish circulation on seawater ϵ_{Nd} has been established by a recent circulation model in the event of a five-fold increase in Nile runoff during the deposition of sapropel S1 (Vadsaria et al., 2019). The model outputs indicate more radiogenic ϵ_{Nd} values (by 2 ϵ_{Nd} units) for deep-water masses associated with a sluggish circulation and a stagnation of deep water, which in turn generate increased boundary-exchange with high-radiogenic material from the east of the EMS. In such a scenario, it has been proposed that ϵ_{Nd} records of the EMS could be related to the degree of stagnation of deep-water in the EMS (Duhamel et al., 2020; Wu et al., 2019).

In Figure 5, we report the ϵ_{Nd} values from EMS and WMS cores and using different symbol for cores located above and below ~1,000 m water. During the S1-period, ϵ_{Nd} obtained at water depth deeper than 1,000 m indicate a contrast between Nd isotopic signature from the EMS and WMS. In the WMS the ϵ_{Nd} values are similar to those of the intermediate water masses indicating an overturning of the circulation. In contrast,

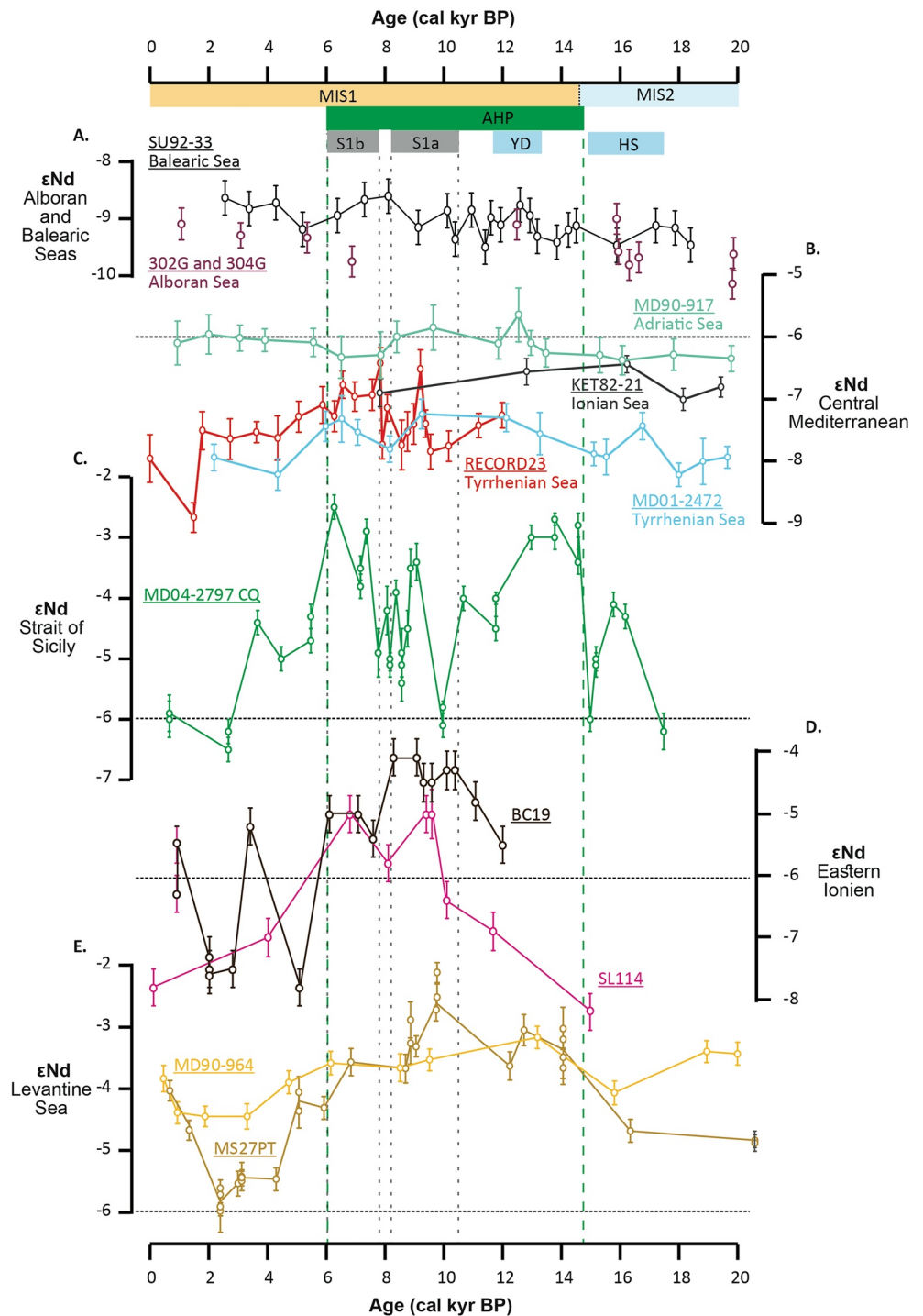


Figure 6. Comparison between ϵNd records obtained in this study (cores MD90-917, KET82-21, RECORD23, and MD01-2472) and previously obtained ϵNd records of the EMS and WMS for the last 20 cal kyr BP: core SU92-33 from Dubois-Dauphin et al. (2017); cores 302G and 304G from Jiménez-Espejo et al. (2015); core MD04-2797CQ from Cornuault et al. (2018); cores BC19 and SL114 from Wu et al. (2019); cores MD90-964 and MS27PT from Duhamel et al. (2020). Also reported are S1a and S1b as defined in Grant et al. (2016), YD and HS1 as defined in Toucanne et al. (2012), AHP as defined in Revel et al. (2010).

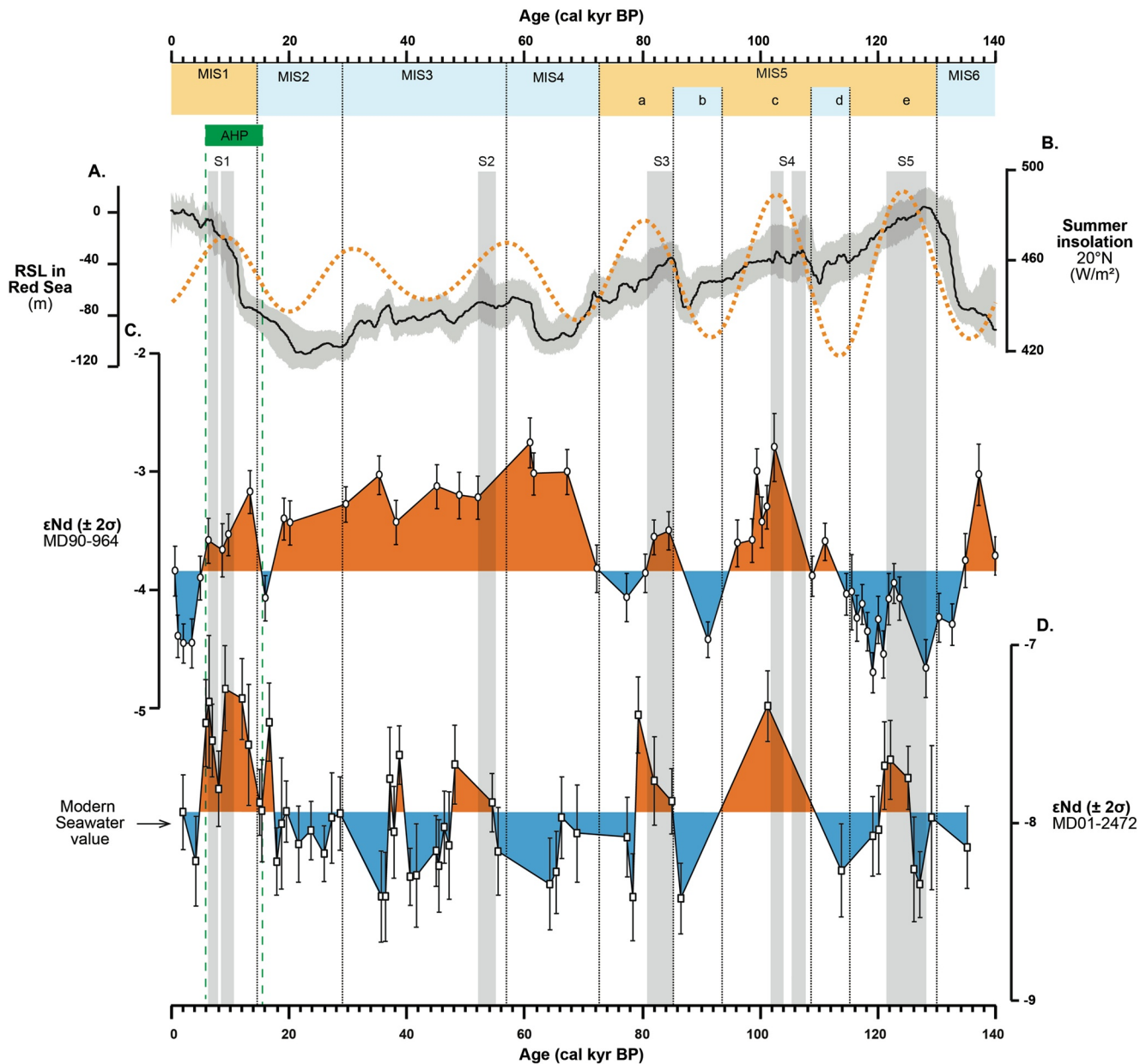


Figure 7. (a) Variations in the Relative Sea Level (RSL) (Grant et al., 2014); (b) summer insolation (June and July) received by the Earth at 20°N (Laskar et al., 2004), calculated using Analyseries software (Paillard et al., 1996); (c) and (d) comparison of ϵNd records obtained from cores MD90-964 (Duhamel et al., 2020) and MD01-2472 (this study), with the ϵNd graphed as variations compared to the core-top value (higher ϵNd values in orange; lower in blue area). Seawater ϵNd value obtained in the northern Tyrrhenian Sea at intermediate water depth (Garcia-Solsona & Jeandel, 2020) has been reported for comparison on y-axis of the curve (d) Sapropel chronology as defined in Zhao et al. (2011) from organic carbon concentration of core MD90-964 sediment.

the ϵNd values of all deep cores from the EMS (below 1,000 m) indicate very radiogenic and homogeneous EMDW. The ϵNd of the EMDW is thus more radiogenic than the LIW which stays relatively unradiogenic. In addition, ϵNd obtained at intermediate depth indicate an west-east gradient through the WMS and EMW which is slightly more radiogenic than the present time ϵNd gradient obtain in seawater (Figure 5). These results can be attributed to a stratification of the water column which isolate the EMDW to the LIW and a strong reduction in water exchange between eastern and western Mediterranean basins with a decrease in the unradiogenic MAW flowing into the deep basin of the EMS compared to the present time.

Nevertheless, Nd isotope differences between the EMS and WMS at intermediate depths during the Holocene are not only related to temporal changes in the Nd isotopic composition of the LIW flowing into the

WMS through the Strait of Sicily. They are also likely to result from mixing changes between radiogenic LIW and overlying (MAW) and underlying (WIW-TDW) unradiogenic water masses, with the intensity of the WIW being mainly controlled by climate-related processes in the Gulf of Lions.

A shift to unradiogenic ϵNd values around 8.2 cal kyr BP at intermediate depths in the Tyrrhenian Sea (Figure 7b) is not observed in deep-waters of the EMS (Figures 7d and 7e). This may reflect (i) a more sluggish ventilation of the EMS at this time, which is not strong enough to modify the Nd isotopic composition of the EMDW that may also be characterized by high Nd concentration due to a long and sustained deep-water stagnation, or (ii) a larger proportion of water masses produced in the western basin (WIW vs. LIW) and flowing in the Tyrrhenian Sea at intermediate depths during cold events centered around 8.2 cal kyr BP. This latter hypothesis is supported by a recovery in the ventilation of the WMS around that time and even earlier (Cacho et al., 2002; Frigola et al., 2007). Additional ϵNd analyses from cores at intermediate depth in the EMS will be necessary to reconstruct the ϵNd variations of the LIW in order to decouple the influence of LIW and WIW through time in the Tyrrhenian Sea. However, ventilation and current velocity records established by Toucanne et al. (2021) at intermediate depth in the Corsica Trough seem to not be link of the intensity of the LIW inflow to the WMS.

5.3. Long-Term Hydrological Variability During the Last Glacial—Interglacial Cycle

Core MD01-2472, located within the modern core of the LIW flowing through the Corsica Trough, allows us to establish, for the first time, the Nd isotopic signature of the intermediate water in the Tyrrhenian Sea over the last climatic cycle (Figure 3e). Long-term variations in the foraminiferal ϵNd of core MD01-2472 display slightly more radiogenic values during intervals of maximum summer (June and July) insolation received by the Earth at 20°N of latitude (Figures 3b and 3e). These time intervals are coeval with past African humid periods (Ehrmann et al., 2013, 2016, 2017; Gasse et al., 2000; Lamb et al., 2018; Revel et al., 2010), corresponding in the EMS to sapropel deposition (S1, S3, S4, and S5) associated with a significant re-organization of the hydrology of the deep and intermediate water masses (e.g., Cramp & O'Sullivan, 1999; Duhamel et al., 2020; Grant et al., 2016; Rossignol-Strick, 1985; Rossignol-Strick et al., 1982; Williams et al., 2015). The foraminiferal ϵNd record obtained in core MD90-964 (33°02.75'N, 32°38.57'E; water depth 1375 m; Figure 1a), located in the eastern Levantine Sea, has been reported for comparison with results obtained in the central Mediterranean Sea (Figures 6c and 6d) (Duhamel et al., 2020). The ϵNd record of core MD90-964 allows us to constrain past changes in the upper EMDW ϵNd over the last climatic cycle. It displays glacial-interglacial variability, with the glacial MIS 6, 4, 3, and 2 displaying more radiogenic values (up to 1.5 ϵNd units) than the interglacial MIS 5 (Figures 5b and 5d) and late MIS 1 (Figure 6). Superimposed on this glacial-interglacial variability, the record indicates precession-forced variability with more radiogenic values during maximum summer insolation of interglacial MIS (Duhamel et al., 2020). Such peak of radiogenic values is coeval to those observed in core MD01-2472 during warm substages of the MIS 5 and the MIS1. Such radiogenic ϵNd values have also been observed during the African humid periods in the early Holocene and during the Eemian in several other EMDW records (Duhamel et al., 2020; Osborne et al., 2010; Scrivner et al., 2004; Wu et al., 2019). EMDW ϵNd maxima during interglacial stages are quite similar, with more radiogenic ϵNd values centered at 121, 101, 80, and 9 cal kyr BP in core MD01-2472 (Figure 6d), which correspond to the timing of long-term African monsoon oscillations controlled by precession-driven insolation changes. In contrast, ϵNd variations observed during the last glacial period (from MIS 4 to MIS 2) are different in the two Mediterranean basins, with more radiogenic ϵNd values (mean value of -3.1 ± 0.2 , $n = 16$; 1σ) recorded in core MD90-964 (Levantine basin) compared to those observed in cores MD01-2472 (Corsica Trough) (Figure 6d) and MD90-912 (south of Sardinia, Figure 3d) (ϵNd values around -8).

It has been proposed that ventilation and current velocity of intermediate water in the Corsica Trough were both higher during glacial MIS and were associated with an increasing contribution of LIW (Toucanne et al., 2012). ϵNd records obtained from cores MD01-2472 and MD90-912 indicate that this cannot be the result of an enhanced inflow of LIW into the WMS, as glacial ϵNd for both cores are not associated with more radiogenic ϵNd compared to interglacial periods.

During its westward flow in the WMS, the radiogenic LIW continuously mixes with surrounding unradiogenic waters lying above and below it. These water masses are the MAW ($\epsilon\text{Nd} = -10.8 \pm 0.4$ to -8.9 ± 0.3 , mean -9.9 ± 0.7 , $n = 15$; 1σ), the WIW ($\epsilon\text{Nd} = -9.2 \pm 0.3$ to -8.0 ± 0.3 , mean -8.7 ± 0.5 , $n = 4$; 1σ) and

the WMDW ($\epsilon\text{Nd} = -9.5 \pm 0.2$ to -8.0 ± 0.3 , mean = -8.9 ± 0.5 , $n = 14$; 1σ) (Dubois-Dauphin et al., 2017; Garcia-Solsona & Jeandel, 2020; Spivack & Wasserburg, 1988; Tachikawa et al., 2004). This induces an ϵNd gradient at intermediate depth between the eastern and western Mediterranean basins, with LIW values becoming progressively more unradiogenic toward the Strait of Sicily (Figure 5) (Tachikawa et al., 2004).

A general circulation model has shown that, compared to the present, periods of low glacial sea level (up to -120 m) may have caused a 50% reduction in water exchange between the North Atlantic and the Mediterranean Sea through the narrow, shallow Gibraltar Strait (Mikolajewicz, 2011). The exchange between the eastern and the western basins of the Mediterranean Sea through the Strait of Sicily was also reduced by 50% during the LGM compared to the Holocene (Grimm et al., 2015; Mikolajewicz, 2011), which may have resulted in a reduction in the inflow of unradiogenic AW in the EMS and in a modification of the ϵNd distribution in the EMS (Cornuault et al., 2018; Wu et al., 2019). More radiogenic upper EMDW has been observed in the Levantine basin during glacial MIS induced by a 50% reduction in the flow of MAW into the EMS (Duhamel et al., 2020). For the LGM, foraminiferal ϵNd values of intermediate and deep cores fit on a straight line indicating a common longitudinal gradient slightly more radiogenic than present day seawater (Figure 5b). This suggests that Mediterranean Sea overturning was still active and was accompanied by a reduction of MAW to the EMS (Figure 5b).

Consequently, the LIW outflow to the WMS would also have been reduced, which could explain the less radiogenic signature of the intermediate water observed in the Tyrrhenian Sea during glacial times. In addition, glacial MIS are associated with colder and more arid climatic conditions which would also induce saltier and cooler MAW circulating in the WMS (Myers et al., 1998; Thunell & Williams, 1989). Hence, convection in the Gulf of Lions is expected to increase at these times, as has been shown in the Alboran and Balearic Seas through slightly lower ϵNd values (Dubois-Dauphin et al., 2017; Jimenez-Espejo et al., 2015) and higher benthic foraminifer $\delta^{13}\text{C}$ (Cacho et al., 2002; Sierro et al., 2005), both of which point to increased production of intermediate and deep waters in the WMS. This is likely to produce mainly unradiogenic ϵNd Winter WIW which flows between the MAW and the LIW. Consequently, during the last glacial period, a weaker inflow of radiogenic LIW from the EMS as well as a likely increase of WIW formation in the Gulf of Lions may have contributed to the decreasing ϵNd of the intermediate water in the Tyrrhenian Sea and the Corsica Trough. However, core MD90-912, located at greater water depth (1,020 m), is associated with more radiogenic ϵNd between 52 and 58 cal kyr BP corresponding to a maximum of summer insolation and the deposition of sapropel S2 in the EMS (Grant et al., 2012; Laskar et al., 2004). It has been demonstrated that the upper EMDW is incorporated into the WMS by overlying LIW as it crosses the Strait of Sicily. This may explain radiogenic values obtained for the deep water south of Sardinia (TDW) as EMDW is more radiogenic particularly during glacial time (Figure 6) (Duhamel et al., 2020).

In the Eastern Mediterranean Basin, several studies have pointed to a sea surface salinity increase during the LGM (Fontugne et al., 1994; Myers et al., 1998; Thunell & Williams, 1989). Models have shown that the formation of deep water in the eastern basin during the LGM was strengthened and occurred principally in the Ionian Sea rather than in the Adriatic Sea as is the case today (Mikolajewicz, 2011). Duhamel et al. (2020) propose that a reduction in the flow of unradiogenic MAW to the Eastern Mediterranean Basin was the main cause of more radiogenic ϵNd values observed for the glacial upper EMDW in the Levantine basin (Figure 6c). Core MD90-917, located in the Adriatic Sea, displays similar values during glacial MIS 2 (-6.3 ± 0.1 ; $n = 4$; 1σ) than the early Holocene (-5.9 ± 0.2 ; $n = 5$; 1σ) (Figure 7b), suggesting that the Adriatic Sea could not have been affected by vertical advection of radiogenic LIW to the EMDW during glacial times. It confirms that the Adriatic Sea was probably not a major production center of deep-water masses in the EMS which was highly radiogenic throughout the deep Levantine basin during glacial MIS 2 (Cornuault et al., 2018; Duhamel et al., 2020).

In contrast, during interglacial MIS 1 and 5, the ϵNd records obtained for intermediate water at the Corsica Trough and the upper EMDW in the Levantine basin systematically display more radiogenic values in phase with the African humid periods (and with the time interval of sapropel deposition) (Figure 6). These periods of radiogenic ϵNd for the upper EMDW and LIW have been associated with an intensification of Nile discharge, a less vigorous circulation of the LIW and a stagnation of EMDW in the EMS, leading to an increase in the contact time between deep-water masses and radiogenic sediments in the EMS margins (Cornuault et al., 2016; Myers, 2002; Myers et al., 1998; Revel et al., 2010, 2014; Tachikawa et al., 2015; Wu et al., 2019).

Such variations in ϵNd observed for the LIW and EMDW are consistent with a circulation model envisaging a five-fold increase in Nile runoff that results in more radiogenic ϵNd for water masses in the EMS (Vadsaria et al., 2019). It has been demonstrated that ventilation and velocity of intermediate water in the Corsica Trough slowed down during interglacial MIS and sapropel deposition (Toucanne et al., 2012) (Figure 3). Comparison of ϵNd records obtained for the Holocene in the central Mediterranean Sea at intermediate depth on both sides of the Strait of Sicily (cores MD01-2472 and MD04-2797; Figures 7b and 7c) suggests that the time interval of moderate radiogenic ϵNd observed during the African humid period (from 14.6 to 6 cal kyr BP) may be linked to an increase in the ϵNd of LIW, which flows from east to west through the Strait, and not to an increase in the intensity of LIW.

The relative variations of MOW bottom-current velocity within the Gulf of Cádiz as reconstructed by Zr/Al from IODP Site U1389 (Bahr et al., 2014, 2015) display inverse variations with the ϵNd record obtained at intermediate depth in the Corsica Trough (MD01-2472) (Figures 3c and 3e). It is well established that MOW intensity within the Gulf of Cádiz is the direct consequence of LIW formation in the EMS (Millet et al., 2006). Each summer insolation maximum is associated with enhanced runoff into the Eastern Mediterranean Sea (Rohling et al., 2015; Rossignol-Strick, 1983), a reduction in LIW formation (Rogerson et al., 2012, 2015) and a reduction in MOW intensity within the Gulf of Cádiz. Our ϵNd record indicates that a more radiogenic signature in the Corsica Trough is associated with reduced MOW intensity, suggesting that such radiogenic values are not linked to an increase in the LIW contribution. Instead, more radiogenic ϵNd values in the Corsica Trough record during summer insolation maximum are probably related to a change of Nd isotopic compositions at the LIW source rather than enhanced advection of LIW into the WMS. It could be then link to a slowdown of LIW formation with more radiogenic ϵNd in agreement with ϵNd records obtained in the Levantine basin.

5.4. Millennial-Scale Variability of the Intermediate Water Masses During the Last Glacial Period and Deglaciation

Planktic and benthic foraminifera $\delta^{18}\text{O}$, benthic foraminifera $\delta^{13}\text{C}$, sortable silt (Toucanne et al., 2012), as well as foraminiferal and ostracod assemblages (Angue Minto'o et al., 2015) were previously studied for core MD01-2472 in order to investigate the impact of rapid climatic changes in the North Atlantic on the ventilation and velocity of the LIW and its subsequent impacts on benthic fauna. The ϵNd record allows us to reconstruct the variability of the water mass sources at intermediate depth in the WMS. Time intervals coeval with Heinrich Stadials HS5, HS4, HS3, and HS1 are associated with slight ϵNd increases (Figure 3). The YD time interval (from 12.8 to 11.5 cal kyr BP) is also associated with radiogenic ϵNd values at intermediate depth in the Corsica Trough (Figure 3). An increase in the deep-current velocity (sortable silt reported in Figure 3) and intermediate water ventilation ($\delta^{13}\text{C}$ of benthic foraminifera reported in Figure 3) at the Corsica Trough has been documented for these time intervals (Toucanne et al., 2012).

The increased iceberg discharges in the North Atlantic during Heinrich Stadial events led to an input of cold freshwater which is believed to be associated with a relative sea level rise between 2 and 40 m (Alley & MacAyeal, 1993; Cutler et al., 2003; Dowdeswell et al., 1995; Hemming, 2004; Lambeck et al., 2003, 2014; Yokoyama et al., 2001). Such freshwater surface Atlantic water inputs to the Mediterranean Sea have been associated with a decrease in SST in the western Mediterranean (Cacho et al., 1999, 2002, 2006; Sierro et al., 2005), which should be associated with a decrease in salinity in the WMS, with the MAW being the main source of comparatively fresh water in the Mediterranean Sea. This has been also associated to a decrease of the deep water salinity in WMDW during HS1, HS3, HS4 and HS5 (Cacho et al., 2006). This decrease in surface salinity may have induced a reduction of deep-water convection in the WMS (Cacho et al., 2006; Sierro et al., 2005). In addition, during low glacial sea level, the relatively fresh MAW input to the EMS was reduced (Mikolajewicz, 2011; Myers et al., 1998) which, combined with marked glacial aridity (Castañeda et al., 2016; Kotthoff et al., 2008; Langgut et al., 2011; Mikolajewicz, 2011; Randlett et al., 2017; Stockhecke et al., 2016), induced an increase in salinity as indicated by data and numerical simulations in the EMS (Béthoux, 1990; Emeis et al., 2000; Mikolajewicz, 2011; Sprovieri et al., 2012; Thunell & Williams, 1989). These conditions induced an active deep and intermediate glacial circulation in the EMS (Cornuault et al., 2016; Duhamel et al., 2020; Grimm et al., 2015; Mikolajewicz, 2011). Accordingly, Heinrich Stadial

events could have led to a decrease in SST (Bartov et al., 2003; Castañeda et al., 2010; Essallami et al., 2007; Rouis-Zargouni et al., 2010; Sprovieri et al., 2012) and enhanced intermediate and deep circulation conditions in the EMS.

Hence, the millennial-scale variability in ϵNd records from the Corsica Trough and the Tyrrhenian Sea, with more radiogenic values in intermediate water (MD01-2472) during Heinrich Stadial events (Figure 3e), could be the result of (1) reduced convection of WIW and WMDW (TDW) during HS events; (2) enhanced input of (i.e., more radiogenic) LIW through the Strait of Sicily induced by a higher sea-level; or (3) the combined effect of these processes. An increasing contribution of LIW to the WMS during time intervals of Heinrich Stadial events is consistent with an increase in ventilation and deep-current velocity at intermediate depth in the Corsica Trough (Toucanne et al., 2012) and an increase in MOW intensity at the Gibraltar Strait where the LIW contributes up to 80% of the MOW volume (Bahr et al., 2015; Llave et al., 2006; Toucanne et al., 2007; Voelker et al., 2006). Such hydrological changes in the Mediterranean basins could play a significant role in triggering a switch from a stadial to an interstadial mode through the MOW injecting saline waters into the northern Atlantic at times of weak AMOC (e.g., Johnson, 1997; Voelker et al., 2006).

6. Conclusions

Foraminiferal ϵNd of sediment cores from the Central Mediterranean Sea allow us to reconstruct past ϵNd variations of LIW and TDW in the WMS, and LIW and upper EMDW in the Ionian and Adriatic Seas documenting hydrological changes in the eastern and western Mediterranean basins since the last glacial time and during the last climatic cycle for the Corsica Trough. Overall, this study provides further constraints on the past hydrology of the two main branches of the LIW that flow into the WMS by establishing continuous ϵNd records at the Corsica Trough and Sardinia Channel. It also provides new constraints on the Nd isotopic composition of deep-water masses formed in the Adriatic Sea.

Comparison between foraminiferal ϵNd records obtained in the Corsica Trough and in the EMS indicates that glacial MIS are associated with an increasing ϵNd gradient between the eastern and western Mediterranean basins at intermediate and deep-water masses. This increasing ϵNd gradient is attributed by limited hydrological connection between both basins related to low sea-level. This is in agreement with previous modeling results (Grimm et al., 2015; Mikolajewicz, 2011). In contrast, intermediate water mass exchange is enhanced between the eastern and western Mediterranean basins during interglacial high sea-level stands when foraminiferal ϵNd records display more radiogenic ϵNd values during the African humid periods (maxima of insolation received by the Earth at low latitude). Our new ϵNd record obtained in the Corsica Trough suggests that periods of high current velocity and ventilation of intermediate water, previously documented in the Corsica Trough, are not linked to higher LIW inflow in the WMS, but rather to increased convection of intermediate and deep-water masses in the WMS (Gulf of Lions). Furthermore, despite the stratification of EMDW, the intermediate circulation from the EMS to the WMS is not reversed during the sapropel S1 deposition. Indeed, both records from the Tyrrhenian Sea display more radiogenic ϵNd during S1 deposition, but with a slight decrease at mid-S1, close to the 8.2 cal kyr BP S1 interruption, synchronous with the less radiogenic ϵNd displayed by cold-water corals that led previous authors to hypothesize a reversal of circulation in the Strait of Sicily (Dubois-Dauphin et al., 2017). These radiogenic seawater ϵNd values are associated with an intensification of Nile discharge, a reduced inflow of Atlantic Water due to reduced exchange between EMS and WMS, a slowdown of the LIW and a stratification of the EMDW (during sapropel deposition). This slowdown of the eastern circulation is then associated with an increase in residence time of deep-water masses in the EMS, which in turn results in a longer contact time between the deep-water masses and the radiogenic sediments along the eastern continental margin of the EMS. Such high radiogenic LIW and upper EMDW can be then propagated to the Tyrrhenian Sea and transferred to both branches of the LIW flowing to the western WMS.

Superimposed on these orbital-scale ϵNd variations, higher ϵNd values are observed during cold Heinrich Stadial events in the Corsica Trough. Such ϵNd variations suggest a reduction of WIW formation in the Gulf of Lions due to freshwater input from the North Atlantic to the WMS and/or the inflow of radiogenic glacial LIW and upper EMDW to the Tyrrhenian Sea, as a result of an active eastern Mediterranean Basin

convection related to saltier and colder conditions. Such pulses of LIW intrusion in the Tyrrhenian Sea are also supported by an increase of the MOW intensity at the Gibraltar Strait.

Data Availability Statement

Data to this article can be found online at <https://doi.org/10.1594/PANGAEA.926899>.

References

Abbott, A. N., Haley, B. A., & McManus, J. (2015). Bottoms up: Sedimentary control of the deep North Pacific Ocean's ϵ Nd signature. *Geology*, 43, 1035. <https://doi.org/10.1130/G37114.1>

Allen, J. R. M., Huntley, B., Brandt, U., Brauer, A., Hubberten, H., Keller, J., et al. (1999). Rapid environmental changes in southern Europe during the last glacial period. *Nature*, 400, 740–743. <https://doi.org/10.1038/23432>

Alley, R. B., & MacAyeal, D. R. (1993). West Antarctic ice sheet collapse: Chimera or clear danger. United States: Antarct. J. United States.

Angue Minto'o, C. M., Bassetti, M. A., Morigi, C., Ducassou, E., Toucanne, S., Jouet, G., & Mulder, T. (2015). Levantine intermediate water hydrodynamic and bottom water ventilation in the northern Tyrrhenian Sea over the past 56,000 years: New insights from benthic foraminifera and ostracods. *Quaternary International*, 357, 295–313. <https://doi.org/10.1016/j.quaint.2014.11.038>

Arbuszewski, J. A., Demenocal, P. B., Clérout, C., Bradtmiller, L., & Mix, A. (2013). Meridional shifts of the Atlantic intertropical convergence zone since the Last Glacial Maximum. *Nature Geoscience*, 6, 959–962. <https://doi.org/10.1038/ngeo1961>

Astraldi, M., Conversano, F., Civitaresse, G., Gasparini, G. P., Ribera d'Alcalà, M., & Vetrano, a. (2002). Water mass properties and chemical signatures in the central Mediterranean region. *Journal of Marine Systems*, 33–34, 155–177. [https://doi.org/10.1016/S0924-7963\(02\)00057-X](https://doi.org/10.1016/S0924-7963(02)00057-X)

Astraldi, M., Gasparini, G. P., Vetrano, A., & Vignudelli, S. (2002). Hydrographic characteristics and interannual variability of water masses in the central Mediterranean: A sensitivity test for long-term changes in the Mediterranean Sea. *Deep Sea Research Part I: Oceanographic Research Papers*, 49, 661–680. [https://doi.org/10.1016/S0967-0637\(01\)00059-0](https://doi.org/10.1016/S0967-0637(01)00059-0)

Ayache, M., Dutay, J.-C., Arsouze, T., Révillon, S., Beuvier, J., & Jeandel, C. (2016). High resolution neodymium characterization along the Mediterranean margins and modeling of ϵ Nd distribution in the Mediterranean basins. *Biogeosciences Discussions*, 1–31. <https://doi.org/10.5194/bg-2016-109>

Bahr, A., Jiménez-Espejo, F. J., Kolasinac, N., Grunert, P., Hernández-Molina, F. J., Röhl, U., et al. (2014). Deciphering bottom current velocity and paleoclimate signals from contourite deposits in the Gulf of Cádiz during the last 140 kyr: An inorganic geochemical approach. *Geochemistry, Geophysics, Geosystems*, 15, 3145–3160. <https://doi.org/10.1002/2014GC005356>

Bahr, A., Kaboth, S., Jiménez-Espejo, F. J., Sierro, F. J., Voelker, A. H. L., Lourens, L., et al. (2015). Persistent monsoonal forcing of Mediterranean Outflow Water dynamics during the late Pleistocene. *Geology*, 43, 951–954. <https://doi.org/10.1130/G37013.1>

Bartov, Y., Goldstein, S. L., Stein, M., & Enzel, Y. (2003). Catastrophic arid episodes in the Eastern Mediterranean linked with the North Atlantic Heinrich events. *Geology*, 31(439). [https://doi.org/10.1130/0091-7613\(2003\)031<0439:CAEITE>2.0.CO;2](https://doi.org/10.1130/0091-7613(2003)031<0439:CAEITE>2.0.CO;2)

Bastian, L., Revel, M., Bayon, G., Dufour, A., & Vigier, N. (2017). Abrupt response of chemical weathering to Late Quaternary hydroclimate changes in northeast Africa. *Scientific Reports*, 7. <https://doi.org/10.1038/srep44231>

Béthoux, J. P., Gentili, B., Raunet, J., & Tailliez, D. (1990). Warming trend in the Western Mediterranean Deep Water. *Nature*, 347, 660–662.

Blanchet, C. L. (2019). A database of marine and terrestrial radiogenic Nd and Sr isotopes for tracing earth-surface processes. *Earth System Science Data*, 11, 741–759. <https://doi.org/10.5194/essd-11-741-2019>

Bout-Roumazeilles, V., Combourieu-Nebout, N., Desprat, S., Siani, G., Turon, J.-L., & Essallami, L. (2013). Tracking atmospheric and riverine terrigenous supplies variability during the last glacial and the Holocene in central Mediterranean. *Climate of the Past*, 9(3), 1065–1087. <https://doi.org/10.5194/cp-9-1065-2013>

Broecker, W. S. (1982). Glacial to interglacial changes in ocean chemistry. *Progress in Oceanography*, 11, 151–197.

Bronk Ramsey, C. (2009). Dealing with outliers and offsets in radiocarbon dating. *Radiocarbon*, 51, 1023–1045. <https://doi.org/10.1017/s00382220003409>

Cacho, I., Grimalt, J. O., Canals, M., Sbaiffi, L., Shackleton, N. J., Schönfeld, J., et al. (2001). Variability of the Western Mediterranean Sea surface temperature during the last 25,000 years and its connection with the Northern Hemisphere climatic changes. *Paleoceanography*, 16, 40–52. <https://doi.org/10.1029/2000PA000502>

Cacho, I., Grimalt, J. O., Sierro, F. J., Shackleton, N., & Canals, M. (2000). Evidence for enhanced Mediterranean thermohaline circulation during rapid climatic coolings. *Earth and Planetary Science Letters*, 183, 417–429. [https://doi.org/10.1016/S0012-821X\(00\)00296-X](https://doi.org/10.1016/S0012-821X(00)00296-X)

Cacho, I., Pelejero, C., Grimalt, J. O., Calafat, A., & Canals, M. (1999). C37 alkenone measurements of sea surface temperature in the Gulf of Lions (NW Mediterranean). *Organic Geochemistry*, 30, 557–566. [https://doi.org/10.1016/S0146-6380\(99\)00038-8](https://doi.org/10.1016/S0146-6380(99)00038-8)

Cacho, I., Shackleton, N., Elderfield, H., Sierro, F. J., & Grimalt, J. O. (2006). Glacial rapid variability in deep-water temperature and $\delta^{18}O$ from the Western Mediterranean Sea. 25(23–24). <https://doi.org/10.1016/j.quascirev.2006.10.004>

Castañeda, I. S., Schefuß, E., Pätzold, J., Damsté, J., Weldeab, S. S., & Schouten, S. (2010). Millennial-scale sea surface temperature changes in the eastern Mediterranean (Nile River Delta region) over the last 27,000 years. *Paleoceanography*, 25, 1208. <https://doi.org/10.1029/2009PA001740>

Castañeda, I. S., Schouten, S., Pätzold, J., Lucassen, F., Kasemann, S., Kuhlmann, H., et al. (2016). Hydroclimate variability in the Nile River Basin during the past 28,000 years. *Earth and Planetary Science Letters*, 438, 47–56. <https://doi.org/10.1016/j.epsl.2015.12.014>

Cheng, X. R., Huang, B. Q., Han, Z. M., Quanhong, Z. H., Tian, J., & Li, J. R. (2005). Foraminiferal isotopic evidence for monsoonal activity in the South China Sea: A present-LGM comparison. *Marine Micropaleontology*, 54, 125–139.

Cita, M. B., Vergnaud-Grazzini, C., Robert, C., Chamley, H., Ciaranfi, N., & d'Onofrio, S. (1977). Paleoclimatic record of a long deep sea core from the eastern Mediterranean. *Quaternary Research*, 8, 205–235.

Copard, K., Colin, C., Douville, E., Freiwald, A., Gudmundsson, G., de Mol, B., et al. (2010). Nd isotopes in deep-sea corals in the North-eastern Atlantic. *Quaternary Science Reviews*, 29, 2499–2508.

Cornuault, M., Tachikawa, K., Vidal, L., Guihou, A., Siani, G., Deschamps, P., et al. (2018). Circulation changes in the eastern Mediterranean Sea over the past 23,000 years inferred from authigenic Nd isotopic ratios. *Paleoceanography and Paleoclimatology*, 33, 264–280. <https://doi.org/10.1002/2017PA003227>

- Cornuault, M., Vidal, L., Tachikawa, K., Licari, L., Rouaud, G., Sonzogni, C., & Revel, M. (2016). Deep water circulation within the eastern Mediterranean Sea over the last 95 kyr: New insights from stable isotopes and benthic foraminiferal assemblages. *Palaeogeography, palaeoclimatology, palaeoecology*, 459, 1–14. <https://doi.org/10.1016/J.PALAEO.2016.06.038>
- Costa, K. M., Russell, J. M., Konecky, B. L., & Lamb, H. F. (2014). Isotopic reconstruction of the African Humid Period and Congo Air Boundary migration at Lake Tana, Ethiopia. *Quaternary Science Reviews*, 83, 58–67.
- Cramp, A., & O'Sullivan, G. (1999). Neogene sapropels in the Mediterranean: A review. *Marine Geology*, 153, 11–28. [https://doi.org/10.1016/S0025-3227\(98\)00092-9](https://doi.org/10.1016/S0025-3227(98)00092-9)
- Cutler, K. B., Edwards, R. L., Taylor, F. W., Cheng, H., Adkins, J., Gallup, C. D., et al. (2003). Rapid sea-level fall and deep-ocean temperature change since the last interglacial period. *Earth and Planetary Science Letters*, 206, 253–271. [https://doi.org/10.1016/S0012-821X\(02\)01107-X](https://doi.org/10.1016/S0012-821X(02)01107-X)
- De Lange, G. J., Thomson, J., Reitz, A., Slomp, C. P., Speranza Principato, M., Erba, E., et al. (2008). Synchronous basin-wide formation and redox-controlled preservation of a Mediterranean sapropel. *Nature Geoscience*, 1, 606–610. <https://doi.org/10.1038/ngeo283>
- DeMenocal, P., Ortiz, J., Guilderson, T., & Sarnthein, M. (2000). Coherent high- and low-latitude climate variability during the holocene warm period. *Science*, 288, 2198–2202. <https://doi.org/10.1126/science.288.5474.2198>
- Dowdeswell, J. A., Maslin, M. A., Andrews, J. T., & McCave, I. N. (1995). Iceberg production, debris rafting, and the extent and thickness of Heinrich layers (H-1, H-2) in North Atlantic sediments. *Geology*, 23, 301–304. [https://doi.org/10.1130/0091-7613\(1995\)023<0297:IPDRAT>2.3.CO;2](https://doi.org/10.1130/0091-7613(1995)023<0297:IPDRAT>2.3.CO;2)
- Du, J., Haley, B. A., Mix, A. C., Walczak, M. H., & Praetorius, S. K. (2018). Flushing of the deep Pacific Ocean and the deglacial rise of atmospheric CO₂ concentrations. *Nature Geoscience*, 11, 749–755. <https://doi.org/10.1038/s41561-018-0205-6>
- Dubois-Dauphin, Q., Montagna, P., Siani, G., Douville, E., Wienberg, C., Hebbeln, D., et al. (2017). Hydrological variations of the intermediate water masses of the western Mediterranean Sea during the past 20 ka inferred from neodymium isotopic composition in foraminifera and cold-water corals. *Climate of the Past*, 13, 17–37. <https://doi.org/10.5194/cp-13-17-2017>
- Duhamel, M., Colin, C., Revel, M., Siani, G., Dapoigny, A., Douville, E., et al. (2020). Variations in eastern Mediterranean hydrology during the last climatic cycle as inferred from neodymium isotopes in foraminifera. *Quaternary Science Reviews*, 237, 106306. <https://doi.org/10.1016/j.quascirev.2020.106306>
- Ehrmann, W., Schmiedl, G., Beuscher, S., & Krüger, S. (2017). Intensity of African humid periods estimated from Saharan Dust fluxes. *PLoS One*, 12, e0170989. <https://doi.org/10.1371/journal.pone.0170989>
- Ehrmann, W., Schmiedl, G., Seidel, M., Krüger, S., & Schulz, H. (2016). A distal 140 kyr sediment record of Nile discharge and East African monsoon variability. *Climate of the Past*, 12, 713–727. <https://doi.org/10.5194/cp-12-713-2016>
- Ehrmann, W., Seidel, M., & Schmiedl, G. (2013). Dynamics of Late Quaternary North African humid periods documented in the clay mineral record of central Aegean Sea sediments. *Global and Planetary Change*, 107, 186–195. <https://doi.org/10.1016/J.GLOPLACHA.2013.05.010>
- Emeis, K.-C., Schulz, H., Struck, U., Rossignol-Strick, M., Erlenkeuser, H., Howell, M. W., et al. (2003). Eastern Mediterranean surface water temperatures and δ¹⁸O composition during deposition of sapropels in the late Quaternary. *Paleoceanography*, 18. <https://doi.org/10.1029/2000PA000617>
- Emeis, K. C., Struck, U., Schulz, H. M., Rosenberg, R., Bernasconi, S., Erlenkeuser, H., et al. (2000). Temperature and salinity variations of Mediterranean Sea surface waters over the last 16,000 years from records of planktonic stable oxygen isotopes and alkenone unsaturation ratios. *Palaeogeography, Palaeoclimatology, Palaeoecology*, 259–280. [https://doi.org/10.1016/S0031-0182\(00\)00053-5](https://doi.org/10.1016/S0031-0182(00)00053-5)
- Essallami, L., Sicre, M. A., Kallel, N., Labeyrie, L., & Siani, G. (2007). Hydrological changes in the Mediterranean Sea over the last 30,000 years. *Geochemistry, Geophysics, Geosystems*, 8. <https://doi.org/10.1029/2007GC001587>
- Filippidi, A., Triantaphyllou, M. V., & De Lange, G. J. (2016). Eastern Mediterranean ventilation variability during sapropel S1 formation, evaluated at two sites influenced by deep-water formation from Adriatic and Aegean Seas. *Quaternary Science Reviews*, 144, 95–106. <https://doi.org/10.1016/j.quascirev.2016.05.024>
- Fontugne, M., Arnold, M., Labeyrie, L., Paterne, M., Calvert, S. E., & Duplessy, J. C. (1994). Paleoenvironment, sapropel chronology and Nile river discharge during the last 20,000 years as indicated by deep-sea sediment records in the eastern Mediterranean. *Radiocarbon*, 34, 75–88.
- Freydier, R., Michard, A., De Lange, G., & Thomson, J. (2001). Nd isotopic compositions of Eastern Mediterranean sediments: Tracers of the Nile influence during sapropel S1 formation? *Marine Geology*, 177, 45–62. [https://doi.org/10.1016/S0025-3227\(01\)00123-2](https://doi.org/10.1016/S0025-3227(01)00123-2)
- Frigola, J., Moreno, A., Cacho, I., Canals, M., Sierro, F. J., Flores, J., et al. (2007). Holocene climate variability in the western Mediterranean region from a deepwater sediment record. *Paleoceanography*, 22, PA2209. <https://doi.org/10.1029/2006PA001307>
- Frigola, J., Moreno, A., Cacho, I., Canals, M., Sierro, F. J., Flores, J. A., & Grimalt, J. O. (2008). Evidence of abrupt changes in Western Mediterranean Deep Water circulation during the last 50kyr: A high-resolution marine record from the Balearic Sea. *Quaternary International*, 181, 88–104. <https://doi.org/10.1016/j.quaint.2007.06.016>
- Garcia-Solsona, E., & Jeandel, C. (2020). Balancing rare earth element distributions in the Northwestern Mediterranean Sea. *Chemical Geology*, 532, 119372. <https://doi.org/10.1016/j.chemgeo.2019.119372>
- Garcin, Y., Melnick, D., Strecker, M. R., Olago, D., & Tiercelin, J.-J. (2012). East African mid-Holocene wet-dry transition recorded in paleo-shorelines of Lake Turkana, northern Kenya Rift. *Earth and Planetary Science Letters*, 331–332, 322–334.
- Gasse, F. (2000). Hydrological changes in the African tropics since the Last Glacial Maximum. *Quaternary Science Reviews*, 189–211. [https://doi.org/10.1016/S0277-3791\(99\)00061-X](https://doi.org/10.1016/S0277-3791(99)00061-X)
- Grant, K. M., Grimm, R., Mikolajewicz, U., Marino, G., Ziegler, M., & Rohling, E. J. (2016). The timing of Mediterranean sapropel deposition relative to insolation, sea-level and African monsoon changes. *Quaternary Science Reviews*, 140, 125–141. <https://doi.org/10.1016/J.QUASCIREV.2016.03.026>
- Grant, K. M., Rohling, E. J., Bar-Matthews, M., Ayalon, A., Medina-Elizalde, M., Ramsey, C. B., et al. (2012). Rapid coupling between ice volume and polar temperature over the past 150,000 years. *Nature*, 491, 744–747. <https://doi.org/10.1038/nature11593>
- Grant, K. M., Rohling, E. J., Bronk Ramsey, C., Cheng, H., Edwards, R. L., Florindo, F., et al. (2014). Sea-level variability over five glacial cycles. *Nature Communications*, 5, 5076.
- Grimm, R., Maier-Reimer, E., Mikolajewicz, U., Schmiedl, G., Müller-Navarra, K., Adloff, F., et al. (2015). Late glacial initiation of Holocene eastern Mediterranean sapropel formation. *Nature Communications*, 6, 7099. <https://doi.org/10.1038/ncomms8099>
- Hemming, S. R. (2004). Heinrich events: Massive late Pleistocene detritus layers of the North Atlantic and their global climate imprint. *Reviews of Geophysics*, 42, RG1005. <https://doi.org/10.1029/2003RG000128>
- Henry, F., Jeandel, C., Dupré, B., & Minster, J.-F. (1994). Particulate and dissolved Nd in the western Mediterranean Sea: Sources, fate and budget. *Marine Chemistry*, 45, 283–305. [https://doi.org/10.1016/0304-4203\(94\)90075-2](https://doi.org/10.1016/0304-4203(94)90075-2)

- Hopkins, T. S. (1988). Recent observations on the intermediate and deep water circulation in the Southern Tyrrhenian Sea. *Oceanologica Acta*, 41–50.
- Jacobsen, S. B., & Wasserburg, G. J. (1980). Sm-Nd isotopic evolution of chondrites. *Earth and Planetary Science Letters*, 50, 139–155. [https://doi.org/10.1016/0012-821X\(80\)90125-9](https://doi.org/10.1016/0012-821X(80)90125-9)
- Jiménez-Espejo, F. J., Pardos-Gené, M., Martínez-Ruiz, F., García-Alix, A., van de Flierdt, T., Toyofuku, T., et al. (2015). Geochemical evidence for intermediate water circulation in the westernmost Mediterranean over the last 20 kyr BP and its impact on the Mediterranean Outflow. *Global and Planetary Change*, 135, 38–46. <https://doi.org/10.1016/j.gloplacha.2015.10.001>
- Johnson, R. G. (1997). Ice age initiation by an ocean-atmospheric circulation change in the Labrador Sea. *Earth and Planetary Science Letters*, 148(1–2), 367–379.
- Kallel, N., Paterne, M., Duplessy, J. C., Vergnaud-Grazzini, C., Pujol, C., Labeyrie, L., et al. (1997). Enhanced rainfall in the Mediterranean region during the last Sapropel Event. *Oceanologica Acta*, 20, 697–712. [https://doi.org/10.1016/S0031-0182\(97\)00021-7](https://doi.org/10.1016/S0031-0182(97)00021-7)
- Kotthoff, U., Müller, U. C., Pross, J., Schmiedl, G., Lawson, I. T., van de Schootbrugge, B., & Schulz, H. (2008). Lateglacial and Holocene vegetation dynamics in the Aegean region: An integrated view based on pollen data from marine and terrestrial archives. *The Holocene*, 18(7), 1019–1032. <https://doi.org/10.1177/0959683608095573>
- Lacan, F., & Jeandel, C. (2005). Neodymium isotopes as a new tool for quantifying exchange fluxes at the continent–ocean interface. *Earth and Planetary Science Letters*, 232, 245–257. <https://doi.org/10.1016/j.epsl.2005.01.004>
- Lamb, H. F., Bates, C. R., Bryant, C. L., Davies, S. J., Huws, D. G., Marshall, M. H., et al. (2018). 150,000-year palaeoclimate record from northern Ethiopia supports early, multiple dispersals of modern humans from Africa. *Scientific Reports*, 8, 1077. <https://doi.org/10.1038/s41598-018-19601-w>
- Lambeck, K., Purcell, A., Johnston, P., Nakada, M., & Yokoyama, Y. (2003). Water-load definition in the glacio-hydro-isostatic sea-level equation. *Quaternary Science Reviews*, 22, 309–318. [https://doi.org/10.1016/S0277-3791\(02\)00142-7](https://doi.org/10.1016/S0277-3791(02)00142-7)
- Lambeck, K., Rouby, H., Purcell, A., Sun, Y., & Sambridge, M. (2014). Sea level and global ice volumes from the Last Glacial Maximum to the Holocene. *Proceedings of the National Academy of Sciences of the United States of America*, 111, 15296–15303. <https://doi.org/10.1073/pnas.1411762111>
- Langgut, D., Almogi-Labin, A., Bar-Matthews, M., & Weinstein-Evron, M. (2011). Vegetation and climate changes in the south eastern Mediterranean during the Last Glacial-Interglacial cycle (86 ka): New marine pollen record. *Quaternary Science Reviews*, 30(27–28), 3960–3972.
- Lascaratos, A., Williams, R. G., & Tragou, E. (1993). A mixed-layer study of the formation of Levantine intermediate water. *Journal of Geophysical Research*, 98, 14739. <https://doi.org/10.1029/93JC00912>
- Laskar, J., Robutel, P., Joutel, F., Gastineau, M., Correia, A. C. M., & Levrard, B. (2004). A long-term numerical solution for the insolation quantities of the Earth. *Astron. Astrophys.*, 428, 261–285. <https://doi.org/10.1051/0004-6361:20041335>
- Lisiecki, L. E., & Raymo, M. E. (2005). A Pliocene-Pleistocene stack of 57 globally distributed benthic $\delta^{18}\text{O}$ records. *Paleoceanography*, 20, PA1003. <https://doi.org/10.1029/2004PA001071>
- Llave, E., Schönfeld, J., Hernández-Molina, F. J., Mulder, T., Somoza, L., Díaz del Río, V., & Sánchez-Almazo, I. (2006). High-resolution stratigraphy of the Mediterranean outflow contourite system in the Gulf of Cadiz during the late Pleistocene: The impact of Heinrich events. *Marine Geology*, 227, 241–262.
- Lugmair, G. W., Shimamura, T., Lewis, R. S., & Anders, E. (1983). Samarium-146 in the early solar system: Evidence from neodymium in the Allende meteorite. *Science*, 222, 1015–1018. <https://doi.org/10.1126/science.222.4627.1015>
- Malanotte-Rizzoli, P., Manca, B. B., D'Alcala, M. R., Theocharis, A., Brenner, S., Budillon, G., et al. (1999). The Eastern Mediterranean in the 80s and in the 90s: The big transition in the intermediate and deep circulations. *Dynamics of Atmospheres and Oceans*, 29, 365–395. [https://doi.org/10.1016/S0377-0265\(99\)00011-1](https://doi.org/10.1016/S0377-0265(99)00011-1)
- Marshall, M. H., Lamb, H. F., Huws, D., Davies, S. J., Bates, C. R., Bloemendal, J., et al. (2011). Late Pleistocene and Holocene drought events at Lake Tana, the source of the Blue Nile. *Global and Planetary Change*, 78, 147–161.
- Martrat, B., Grimalt, J. O., Lopez-Martinez, C., Cacho, I., Sierro, F. J., Flores, J. A., et al. (2004). Abrupt temperature changes in the Western Mediterranean over the past 250,000 years. *Science*, 306, 1762–1765.
- Melki, T., Kallel, N., Jorissen, F. J., Guichard, F., Dennielou, B., Berné, S., et al. (2009). Abrupt climate change, sea surface salinity and paleoproductivity in the western Mediterranean Sea (Gulf of Lion) during the last 28 kyr. *Palaeogeography, Palaeoclimatology, Palaeoecology*, 279, 96–113. <https://doi.org/10.1016/j.palaeo.2009.05.005>
- Menot, G., Pivot, S., Bouloubassi, I., Davtian, N., Hennekam, R., Bosch, D., et al. (2020). Timing and stepwise transitions of the African Humid Period from geochemical proxies in the Nile deep-sea fan sediments. *Quaternary Science Reviews*, 228.
- Mercone, D., Thomson, J., Croudace, I. W., Siani, G., Paterne, M., Troelstra, S., et al. (2000). Duration of S1, the most recent sapropel in the eastern Mediterranean Sea, as indicated by accelerator mass spectrometry radiocarbon and geochemical evidence. *Paleoceanography*, 15, 336–347. <https://doi.org/10.1029/1999PA000397>
- Mikolajewicz, U. (2011). Modeling Mediterranean Ocean climate of the last glacial maximum. *Climate of the Past*, 7, 161–180. <https://doi.org/10.5194/cp-7-161-2011>
- Millot, C. (1999). Circulation in the western Mediterranean Sea. *Journal of Marine Systems*, 20, 423–442. [https://doi.org/10.1016/S0924-7963\(98\)00078-5](https://doi.org/10.1016/S0924-7963(98)00078-5)
- Millot, C., Candela, J., Fuda, J.-L., & Tber, Y. (2006). Large warming and salinification of the Mediterranean outflow due to changes in its composition. *Deep-Sea Research Part I Oceanographic Research Papers*, 53, 656–666. <https://doi.org/10.1016/j.dsr.2005.12.017>
- Millot, C., & Taupier-Letage, I. (2005). Circulation in the Mediterranean Sea. *Environmental Chemistry*, 5, 29–66. <https://doi.org/10.1007/b107143>
- Montero-Serrano, J.-C., Frank, N., Tisnérat-Laborde, N., Colin, C., Wu, C.-C., Lin, K., et al. (2013). Decadal changes in the mid-depth water mass dynamic of the Northeastern Atlantic margin (Bay of Biscay). *Earth and Planetary Science Letters*, 364, 134–144. <https://doi.org/10.1016/J.EPSL.2013.01.012>
- Moreno, A., Cacho, I., Canals, M., Grimalt, J. O., Sánchez-Goñi, M. F., Shackleton, N., et al. (2005). Links between marine and atmospheric processes oscillating on a millennial time-scale. A multi-proxy study of the last 50,000 yr from the Alboran Sea (Western Mediterranean Sea). *Quaternary Science Reviews*, 24, 1623–1636. <https://doi.org/10.1016/j.quascirev.2004.06.018>
- Moreno, A., Cacho, I., Canals, M., Prins, M. a., Sánchez-Goñi, M.-F., Grimalt, O. J., et al. (2002). Saharan dust transport and high-latitude glacial climatic variability: The Alboran Sea record. *Quaternary Research*, 58, 318–328. <https://doi.org/10.1006/qres.2002.2383>
- Myers, P. G., Haines, K., & Rohling, E. J. (1998). Modeling the paleocirculation of the Mediterranean: The Last Glacial Maximum and the Holocene with emphasis on the formation of sapropel S1. *Paleoceanography*, 13, 586–606. <https://doi.org/10.1029/98PA02736>

- O'Nions, R. K., Hamilton, P. J., & Evensen, N. M. (1977). Variations in $^{143}\text{Nd}/^{144}\text{Nd}$ and $^{87}\text{Sr}/^{86}\text{Sr}$ ratios in oceanic basalts. *Earth and Planetary Science Letters*, *34*, 13–22.
- Osborne, A. H., Marino, G., Vance, D., & Rohling, E. J. (2010). Eastern Mediterranean surface water Nd during Eemian sapropel S5: Monitoring northerly (mid-latitude) versus southerly (sub-tropical) freshwater contributions. *Quaternary Science Reviews*, *29*, 2473–2483.
- Paillard, D., Labeyrie, L., & Yiou, P. (1996). Analyseries 1.0: A Macintosh software for the analysis of geographical timeseries. *Eos, Transactions AGU*, *77*, 379.
- Paterne, M., Kallel, N., Labeyrie, L., Vautravers, M., Duplessy, J.-C., Rossignol-Strick, M., et al. (1999). Hydrological relationship between the North Atlantic Ocean and the Mediterranean Sea during the past 15–75 kyr. *Paleoceanography*, *14*, 626–638. <https://doi.org/10.1029/1998PA900022>
- Penaud, A., Eynaud, F., Voelker, A., Kageyama, M., Marret, F., Turon, J. L., et al. (2011). Assessment of sea surface temperature changes in the Gulf of Cadiz during the last 30 ka: Implications for glacial changes in the regional hydrography. *Biogeosciences*, *8*, 2295–2316. <https://doi.org/10.5194/bg-8-2295-2011>
- Piotrowski, A. M., Galy, A., Nicholl, J. L., Roberts, N. L., Wilson, D. J., Clegg, J., et al. (2012). Reconstructing deglacial North and South Atlantic deep water sourcing using foraminiferal Nd isotopes. *Earth and Planetary Science Letters*, *357–358*, 289–297. <https://doi.org/10.1016/j.epsl.2012.09.036>
- Randlett, M.-E., Bechtel, A., vander Meer, M. T. J., Peterse, F., Litt, T., Pickarski, N., et al. (2017). Biomarkers in Lake Van sediments reveal dry conditions in eastern Anatolia during 10,000–10,000 years B.P., *Geochemistry, Geophysics, Geosystems*, *18*, 571–583. <https://doi.org/10.1002/2016GC006621>
- Reimer, P. J., Austin, W. E. N., Bard, E., Bayliss, A., Blackwell, P. G., Bronk Ramsey, C., et al. (2020). The INTCAL20 Northern hemisphere radiocarbon age calibration curve (0–55 Cal kyr BP). *Radiocarbon*, 1–33. <https://doi.org/10.1017/rdc.2020.41>
- Revel, M., Ducassou, E., Grousset, F. E., Bernasconi, S. M., Migeon, S., Revillon, S., et al. (2010). 100,000 Years of African monsoon variability recorded in sediments of the Nile margin. *Quaternary Science Reviews*, *29*, 1342–1362. <https://doi.org/10.1016/j.quascirev.2010.02.006>
- Roberts, N. L., Piotrowski, A. M., Elderfield, H., Eglinton, T. I., & Lomas, M. W. (2012). Rare earth element association with foraminifera. *Geochimica Cosmochimica Acta*, *94*, 57–71. <https://doi.org/10.1016/j.gca.2012.07.009>
- Robinson, A. R., Leslie, W. G., Theocharis, A., & Lascaratos, A. (2001). Mediterranean Sea circulation. *Ocean Currents*, *1*, 19.
- Roether, W., Manca, B. B., Klein, B., Bregant, D., Georgopoulos, D., Beitzel, V., et al. (1996). Recent changes in eastern Mediterranean deep waters. *Science*, *271*, 333. <https://doi.org/10.1126/science.271.5247.333>
- Rogerson, M., Colmenero-Hidalgo, E., Levine, R. C., Rohling, E. J., Voelker, A. H. L., Bigg, G. R., et al. (2010). Enhanced Mediterranean-Atlantic exchange during Atlantic freshening phases. *Geochemistry, Geophysics, Geosystems*, *11*, Q08013.
- Rogerson, M., Rohling, E. J., Bigg, G. R., & Ramirez, J. (2012). Paleoceanography of the Atlantic-Mediterranean exchange: Overview and first quantitative assessment of climatic forcing. *Reviews of Geophysics*, *50*, RG2003. <https://doi.org/10.1029/2011RG000376>
- Rogerson, M., Rohling, E. J., Weaver, P. P. E., & Murray, J. W. (2005). Glacial to interglacial changes in the settling depth of the Mediterranean Outflow plume. *Paleoceanography*, *20*, PA3007. <https://doi.org/10.1029/2004PA001106>
- Rohling, E. J. (1994). Review and new aspects concerning the formation of eastern Mediterranean sapropels. *Marine Geology*, *122*, 1–28. [https://doi.org/10.1016/0025-3227\(94\)90202-X](https://doi.org/10.1016/0025-3227(94)90202-X)
- Rohling, E. J., Cane, T. R., Bouloubassi, I., Kemp, A. E. S., Kroon, D., Schiebel, R., et al. (2002). African monsoon variability during the previous interglacial maximum. *Earth and Planetary Science Letters*, *202*, 61–75. [https://doi.org/10.1016/S0012-821X\(02\)00775-6](https://doi.org/10.1016/S0012-821X(02)00775-6)
- Rohling, E. J., Den Dulk, M., Pujol, C., & Vergnaud-Grazzini, C. (1995). Abrupt hydrographic change in the Alboran Sea (western Mediterranean) around 8000 yrs BP. *Deep-Sea Research Part I Oceanographic Research Paper*, *42*, 1609–1619. [https://doi.org/10.1016/0967-0637\(95\)00069-1](https://doi.org/10.1016/0967-0637(95)00069-1)
- Rohling, E. J., Jorissen, F. J., & De Stigter, H. C. (1997). 200 Years interruption of Holocene sapropel formation in the Adriatic Sea. *Journal of Micropalaeontology*, *16*, 97–108. <https://doi.org/10.1144/jm.16.2.97>
- Rohling, E. J., Marino, G., & Grant, K. M. (2015). Mediterranean climate and oceanography, and the periodic development of anoxic events (sapropels). *Earth-Science Reviews*, *143*, 62–97. <https://doi.org/10.1016/j.earscirev.2015.01.008>
- Rossignol-Strick, M. (1985). Mediterranean Quaternary sapropels, an immediate response of the African monsoon to variation of insolation. *Palaeogeography, Palaeoclimatology, Palaeoecology*, *49*, 237–263.
- Rossignol-Strick, M., Nesteroff, W., Olive, P., & Vergnaud-Grazzini, C. (1982). After the deluge: Mediterranean stagnation and sapropel formation. *Nature*, *285*, 105–110. <https://doi.org/10.1038/295105a0>
- Rouis-Zargouni, I., Turon, J.-L., Londeix, L., Essallami, L., Kallel, N., & Sicre, M.-A. (2010). Environmental and climatic changes in the central Mediterranean Sea (Siculo-Tunisian Strait) during the last 30ka based on dinoflagellate cyst and planktonic foraminifera assemblages. *Palaeogeography, Palaeoclimatology, Palaeoecology*, *285*(1–2), 17–29. <https://doi.org/10.1016/j.palaeo.2009.10.015>
- Rousseau, T. C. C., Sonke, J. E., Chmieleff, J., van Beek, P., Souhaut, M., Boaventura, G., et al. (2015). Rapid neodymium release to marine waters from lithogenic sediments in the Amazon estuary. *Nature Communications*, *6*, 7592. <https://doi.org/10.1038/ncomms8592>
- Sammari, C., Millot, C., Taupier-Letage, I., Stefani, A., & Brahim, M. (1999). Hydrological characteristics in the Tunisia-Sardinia-Sicily area during spring 1995. *Deep-Sea Research Part I: Oceanographic Research Paper*, *46*, 1671–1703. [https://doi.org/10.1016/S0967-0637\(99\)00026-6](https://doi.org/10.1016/S0967-0637(99)00026-6)
- Scheuvs, D., Schütz, L., Kandler, K., Ebert, M., & Weinbruch, S. (2013). Bulk composition of northern African dust and its source sediments—A compilation. *Earth-Science Reviews*, *116*, 170–194. <https://doi.org/10.1016/j.earscirev.2012.08.005>
- Schlitzer, R. (2018). *Ocean Data View*. <https://odv.awi.de>
- Schmiedl, G., Kuhnt, T., Ehrmann, W., Emeis, K.-C. C., Hamann, Y., Kotthoff, U., et al. (2010). Climatic forcing of eastern Mediterranean deep-water formation and benthic ecosystems during the past 22 000 years. *Quaternary Science Reviews*, *29*, 3006–3020. <https://doi.org/10.1016/j.quascirev.2010.07.002>
- Schmiedl, G., Mitschele, A., Beck, S., Emeis, K.-C., Hemleben, C., Schulz, H., et al. (2003). Benthic foraminiferal record of ecosystem variability in the eastern Mediterranean Sea during times of sapropel S5 and S6 deposition. *Palaeogeography, Palaeoclimatology, Palaeoecology*, *190*, 139–164. [https://doi.org/10.1016/S0031-0182\(02\)00603-X](https://doi.org/10.1016/S0031-0182(02)00603-X)
- Schroeder, K., Garcia-Lafuente, J., Josey, S. A., Artale, V., Buongiorno Nardelli, B., Carrillo, A., & Lionello, P. (2012). Circulation of the Mediterranean Sea and its variability. In *The climate of the mediterranean region: From the past to the future*. Elsevier. 187–256, 2012, 978-0-12-416042-2.
- Schroeder, K., Gasparini, G. P., Tangherlini, M., & Astraldi, M. (2006). Deep and intermediate water in the western Mediterranean under the influence of the Eastern Mediterranean Transient. *Geophysical Research Letters*, *33*, L21607. <https://doi.org/10.1029/2006GL027121>
- Scrivner, A. E., Vance, D., & Rohling, E. J. (2004). New neodymium isotope data quantify Nile involvement in Mediterranean anoxic episodes. *Geology*, *32*, 565. <https://doi.org/10.1130/G20419.1>

- Shanahan, T. M., McKay, N. P., Hughen, K. A., Overpeck, J. T., Otto-Bliesner, B., Heil, C. W., et al. (2015). The time-transgressive termination of the African Humid Period. *Nature Geoscience*, 8, 140–144. <https://doi.org/10.1038/ngeo2329>
- Siani, G., Paterne, M., Arnold, M., Bard, E., Métiévier, B., Tisnerat, N., et al. (2000). Radiocarbon reservoir ages in the Mediterranean Sea and Black Sea. *Radiocarbon*, 42, 271–280. <https://doi.org/10.1017/S003822200059075>
- Siani, G., Magny, M., Paterne, M., Debret, M., & Fontugne, M. (2013). Paleohydrology reconstruction and Holocene climate variability in the South Adriatic Sea. *Climate of the Past*, 9, 499–515. <https://doi.org/10.5194/cp-9-499-2013>
- Siani, G., Paterne, M., & Colin, C. (2010). Late glacial to Holocene planktic foraminifera bioevents and climatic record in the South Adriatic Sea. *Journal of Quaternary Science*, 25, 808–821. <https://doi.org/10.1002/jqs.1360>
- Siani, G., Paterne, M., Michel, E., Sulpizio, R., Sbrana, A., Arnold, M., et al. (2001). Mediterranean Sea surface radiocarbon reservoir age changes since the last glacial maximum. *Science*, 80(294), 1917–1920. <https://doi.org/10.1126/science.1063649>
- Siani, G., Sulpizio, R., Paterne, M., & Sbrana, A. (2004). Tephrostratigraphy study for the last 18,000 C years in a deep-sea sediment sequence for the South Adriatic. *Quaternary Science Reviews*, 23, 2485–2500.
- Sicre, M.-A., Siani, G., Genty, D., Kallel, N., & Essallami, L. (2013). Seemingly divergent sea surface temperature proxy records in the central Mediterranean during the last deglaciation. *Climate of the Past*, 9, 1375–1383. <https://doi.org/10.5194/cp-9-1375-2013>
- Siddall, M., Khattiwala, S., van de Flierdt, T., Jones, K., Goldstein, S. L., Hemming, S. R., et al. (2008). Toward explaining the Nd paradox using reversible scavenging in an ocean general circulation model. *Earth and Planetary Science Letters*, 274, 448–461. <https://doi.org/10.1016/j.epsl.2008.07.044>
- Sierro, F. J., Hodell, D. A., Curtis, J. H., Flores, J. A., Reguera, I., Colmenero-Hidalgo, E., et al. (2005). Impact of iceberg melting on Mediterranean thermohaline circulation during Heinrich events. *Paleoceanography*, 20. <https://doi.org/10.1029/2004PA001051>
- Skinner, L. C., Sadekov, A., Brandon, M., Greaves, M., Plancherel, Y., de la Fuente, M., et al. (2019). Rare Earth Elements in early-diagenetic foraminifer ‘coatings’: Pore-water controls and potential palaeoceanographic applications. *Geochimica et Cosmochimica Acta*, 245, 118–132.
- Skonieczny, C., McGee, D., Winckler, G., Bory, A., Bradtmiller, L. I., Kinsley, C. W., et al. (2019). Monsoon-driven Saharan dust variability over the past 240,000 years. *Science Advances*, 5. <https://doi.org/10.1126/sciadv.aav1887>
- Spivack, A. J., & Wasserburg, G. J. (1988). Neodymium isotopic composition of the Mediterranean outflow and the eastern North Atlantic. *Geochimica et Cosmochimica Acta*, 52, 2767–2773. [https://doi.org/10.1016/0016-7037\(88\)90144-5](https://doi.org/10.1016/0016-7037(88)90144-5)
- Sprovieri, M., Di Stefano, E., Incarbona, A., Salvaggio Manta, D., Pelosi, N., Ribera d’Alcalà, M., & Sprovieri, R. (2012). Centennial- to millennial-scale climate oscillations in the Central-Eastern Mediterranean Sea between 20,000 and 70,000 years ago: Evidence from a high-resolution geochemical and micropaleontological record. *Quaternary Science Reviews*, 46, 126–135. <https://doi.org/10.1016/J.QUASCIREV.2012.05.005>
- Stichel, T., Hartman, A. E., Duggan, B., Goldstein, S. L., Scher, H., & Pahnke, K. (2015). Separating biogeochemical cycling of neodymium from water mass mixing in the Eastern North Atlantic. *Earth and Planetary Science Letters*, 412, 245–260.
- Stockhecke, M., Timmermann, A., Kipfer, R., Haug, G. H., Kwiciczen, T., Friedrich, L., et al. (2016). Millennial to orbital-scale variations of drought intensity in the Eastern Mediterranean. *Quaternary Science Reviews*, 133, 77–95.
- Tachikawa, K., Athias, V., & Jeandel, C. (2003). Neodymium budget in the modern ocean and paleo-oceanographic implications. *Journal of Geophysical Research*, 108, 3254. <https://doi.org/10.1029/1999JC000285>
- Tachikawa, K., Piotrowski, A. M., & Bayon, G. (2014). Neodymium associated with foraminiferal carbonate as a recorder of seawater isotopic signatures. *Quaternary Science Reviews*, 88, 1–13. <https://doi.org/10.1016/j.quascirev.2013.12.027>
- Tachikawa, K., Roy-Barman, M., Michard, A., Thouron, D., Yeghicheyan, D., & Jeandel, C. (2004). Neodymium isotopes in the Mediterranean Sea: Comparison between seawater and sediment signals. *Geochimica et Cosmochimica Acta*, 68, 3095–3106. <https://doi.org/10.1016/j.gca.2004.01.024>
- Tachikawa, K., Toyofuku, T., Basile-Doelsch, I., & Delhay, T. (2013). Microscale neodymium distribution in sedimentary planktonic foraminiferal tests and associated mineral phases. *Geochimica et Cosmochimica Acta*, 100, 11–23. <https://doi.org/10.1016/j.gca.2012.10.010>
- Tachikawa, K., Vidal, L., Cornuault, M., Garcia, M., Pothin, A., Sonzogni, C., et al. (2015). Eastern Mediterranean Sea circulation inferred from the conditions of S1 sapropel deposition. *Climate of the Past*, 11, 855–867. <https://doi.org/10.5194/cp-11-855-2015>
- Taviani, M., Angeletti, L., Canese, S., Cannas, R., Cardone, F., Cau, A., et al. (2015). The “Sardinian cold-water coral province” in the context of the Mediterranean coral ecosystems. *Deep Sea Research Part II: Topical Studies in Oceanography*, 145, 61–78. <https://doi.org/10.1016/j.dsr2.2015.12.008>
- Tesi, T., Asioli, A., Minisini, D., Maselli, V., Dalla Valle, G., Gamberi, F., et al. (2017). Large-scale response of the Eastern Mediterranean thermohaline circulation to African monsoon intensification during sapropel S1 formation. *Quaternary Science Reviews*, 159, 139–154. <https://doi.org/10.1016/j.quascirev.2017.01.020>
- Thunell, R. C., & Williams, D. F. (1989). Glacial–Holocene salinity changes in the Mediterranean Sea: Hydrographic and depositional effects. *Nature*, 338, 493–496. <https://doi.org/10.1038/338493a0>
- Toucanne, S., Angue Minto’o, C. M., Fontanier, C., Bassetti, M. A., Jorry, S. J., & Jouet, G. (2015). Tracking rainfall in the northern Mediterranean borderlands during sapropel deposition. *Quaternary Science Reviews*, 129, 178–195. <https://doi.org/10.1016/j.quascirev.2015.10.016>
- Toucanne, S., Jouet, G., Ducassou, E., Bassetti, M. A., Dennielou, B., Angue Minto’o, C. M., et al. (2012). A 130,000-year record of Levantine Intermediate Water flow variability in the Corsica Trough, western Mediterranean Sea. *Quaternary Science Reviews*, 33, 55–73. <https://doi.org/10.1016/j.quascirev.2011.11.020>
- Toucanne, S., Mulder, T., Schönfeld, J., Hanquiez, V., Gonthier, E., Duprat, J., et al. (2007). Contourites of the Gulf of Cadiz: A high-resolution record of the paleocirculation of the Mediterranean outflow water during the last 50,000 years. *Palaeogeography, Palaeoclimatology, Palaeoecology*, 246, 354–366.
- Vadsaria, T., Ramstein, G., Dutay, J.-C., Li, L., Ayache, & M., & Richon, C. (2019). Simulating the occurrence of the last sapropel event (S1): Mediterranean basin ocean dynamics simulations using Nd isotopic composition modeling. *Paleoceanography and Paleoclimatology*, 34, 237–251. <https://doi.org/10.1029/2019PA003566>
- Vance, D., Scrivner, A. E., & Beney, P. (2004). The use of foraminifera as a record of the past neodymium isotope composition of seawater. *Paleoceanography*, 19, PA2009. <https://doi.org/10.1029/2003PA000957>
- Voelker, A. H. L., Lebreiro, S. M., Schönfeld, J., Cacho, I., Erlenkeuser, H., & Abrantes, F. (2006). Mediterranean outflow strengthening during northern hemisphere coolings: A salt source for the glacial Atlantic? *Earth and Planetary Science Letters*, 245, 39–55. <https://doi.org/10.1016/J.EPSL.2006.03.014>
- von Grafenstein, U., Erlenkeuser, H., Müller, J., Jouzel, J., & Johnsen, S. (1998). The cold event 8200 years ago documented in oxygen isotope records of precipitation in Europe and Greenland. *Climate Dynamics*, 14, 73–81. <https://doi.org/10.1007/s003820050210>

- Weldeab, S., Emeis, K.-C., Hemleben, C., Vennemann, T. W., & Schulz, H. (2002). Sr and Nd isotope composition of Late Pleistocene sapropels and nonsapropelic sediments from the Eastern Mediterranean Sea: Implications for detrital influx and climatic conditions in the source areas. *Geochimica et Cosmochimica Acta*, 66, 3585–3598. [https://doi.org/10.1016/S0016-7037\(02\)00954-7](https://doi.org/10.1016/S0016-7037(02)00954-7)
- Williams, D. F., & Thunell, R. C. (1979). Faunal and oxygen isotopic evidence for surface water salinity changes during sapropel formation in the eastern Mediterranean. *Sedimentary Geology*, 23, 81–93. [https://doi.org/10.1016/0037-0738\(79\)90007-1](https://doi.org/10.1016/0037-0738(79)90007-1)
- Williams, M. A. J., Duller, G. A. T., Williams, F. M., Woodward, J. C., Macklin, M. G., El Tom, O. A. M., et al. (2015). Causal links between Nile floods and eastern Mediterranean sapropel formation during the past 125 kyr confirmed by OSL and radiocarbon dating of Blue and White Nile sediments. *Quaternary Science Reviews*, 130, 89–108. <https://doi.org/10.1016/J.QUASCIREV.2015.05.024>
- Wilson, D. J., Piotrowski, A. M., Galy, A., & Clegg, J. A. (2013). Reactivity of neodymium carriers in deep sea sediments: Implications for boundary exchange and paleoceanography. *Geochimica et Cosmochimica Acta*, 109, 197–221.
- Wu, J., Pahnke, K., Böning, P., Wu, L., Michard, A., & de Lange, G. J. (2019). Divergent Mediterranean seawater circulation during Holocene sapropel formation – Reconstructed using Nd isotopes in fish debris and foraminifera. *Earth and Planetary Science Letters*, 511, 141–153. <https://doi.org/10.1016/J.EPSL.2019.01.036>
- Wu, Q., Colin, C., Liu, Z., Thil, F., Dubois-Dauphin, Q., Frank, N., et al. (2015). Neodymium isotopic composition in foraminifera and authigenic phases of the South China Sea sediments: Implications for the hydrology of the North Pacific Ocean over the past 25 kyr. *Geochemistry, Geophysics, Geosystems*, 16, 3883–3904. <https://doi.org/10.1002/2015GC005871>
- Xu, Z., Li, T., Colin, C., Clift, P. D., Sun, R., Yu, Z., et al. (2018). Seasonal variations in the siliciclastic fluxes to the Western Philippine Sea and their impacts on seawater ϵ_{Nd} values inferred from 1 year of in situ observations above Benham rise. *Journal of Geophysical Research Oceans*, 123, 6688–6702. <https://doi.org/10.1029/2018JC014274>
- Yokoyama, Y., Esat, T. M., & Lambeck, K. (2001). Coupled climate and sea-level changes deduced from Huon Peninsula coral terraces of the last ice age. *Earth and Planetary Science Letters*, 193, 579–587. [https://doi.org/10.1016/S0012-821X\(01\)00515-5](https://doi.org/10.1016/S0012-821X(01)00515-5)
- Yu, Z., Colin, C., Ma, R., Meynadier, L., Wan, S., Wu, Q., et al. (2018). Antarctic Intermediate Water penetration into the Northern Indian Ocean during the last deglaciation. *Earth and Planetary Science Letters*, 500, 67–75. <https://doi.org/10.1016/J.EPSL.2018.08.006>
- Zhao, Y., Colin, C., Liu, Z., Paterne, M., Siani, G., & Xie, X. (2012). Reconstructing precipitation changes in northeastern Africa during the Quaternary by clay mineralogical and geochemical investigations of Nile deep-sea fan sediments. *Quaternary Science Reviews*, 57, 58–70. <https://doi.org/10.1016/J.QUASCIREV.2012.10.009>
- Zhao, Y., Liu, Z., Colin, C., Paterne, M., Siani, G., Cheng, X., et al. (2011). Variations of the Nile suspended discharges during the last 1.75 Myr. *Palaeogeography, Palaeoclimatology, Palaeoecology*, 311, 230–241. <https://doi.org/10.1016/J.PALAEO.2011.09.001>
- Zirks, E., Krom, M. D., Zhu, D., Schmiedl, G., & Goodman-Tchernov, B. N. (2019). Evidence for the presence of oxygen-depleted sapropel intermediate water across the Eastern Mediterranean during Sapropel S1. *ACS Earth and Space Chemistry*.